AN EXPERIMENTAL STUDY OF THE MOBILITY OF EDGE DISLOCATIONS IN PURE COPPER SINGLE CRYSTALS

Thesis by

Kenneth Mark Jassby

In Partial Fulfillment of the Requirements
For the Degree of
Doctor of Philosophy

California Institute of Technology
Pasadena, California
1970

(Submitted July 7, 1969)

To my Mother, and
In memory of my Father

ACKNOWLEDGMENTS

The author is much indebted to Professor Thad Vreeland, Jr. for his untiring guidance throughout the duration of the work described in this thesis. Thanks are extended to Professor D. S. Wood for providing insight into several of the experimental problems. The author's work was greatly expedited by the research of several graduate students who preceded him. In this vein, appreciation is extended to Drs. R. C. Blish, J. A. Gorman, D. P. Pope, and A. P. L. Turner.

The Central Machine Shop of the California Institute of Technology, and especially Mr. Norman Keidel, provided excellent engineering services.

Fellowship support from the National Research Council of Canada throughout the course of this work is gratefully acknowledged. In addition, the author wishes to thank the California Institute of Technology for several tuition scholarships.

It is a pleasure for the author to thank Mrs. Roberta Duffy for typing the thesis.

ABSTRACT

The velocity of selectively-introduced edge dislocations in 99.999 percent pure copper crystals has been measured as a function of stress at temperatures from 66°K to 373°K by means of a torsion technique. The range of resolved shear stress was 0 to 15 megadynes/cm^2 for seven temperatures (66°K, 74°K, 83°K, 123°K, 173°K, 296°K, 373°K).

Dislocation mobility is characterized by two distinct features; (a) relatively high velocity at low stress (maximum velocities of about 9000 cm/sec were realized at low temperatures), and (b) increasing velocity with decreasing temperature at constant stress.

The relation between dislocation velocity and resolved shear stress is:

$$v = v_o\left(\frac{\tau_r}{\tau_o}\right)^n$$

where v is the dislocation velocity at resolved shear stress τ_r, v_o is a constant velocity chosen equal to 2000 cm/sec, τ_o is the resolved shear stress required to maintain velocity v_o, and n is the mobility coefficient. The experimental results indicate that τ_o decreases from 16.3×10^6 to 3.3×10^6 dynes/cm^2 and n increases from about 0.9 to 1.1 as the temperature is lowered from 296°K to 66°K.

The experimental dislocation behavior is consistent with an interpretation on the basis of phonon drag. However, the complete temperature dependence of dislocation mobility could not be closely approximated by the predictions of one or a combination of mechanisms.

TABLE OF CONTENTS

LIST OF TABLES

LIST OF FIGURES

AN EXPERIMENTAL STUDY OF THE MOBILITY OF EDGE DISLOCATIONS IN PURE COPPER SINGLE CRYSTALS

I. INTRODUCTION

The experimental study of dislocation mobility in single crystals has advanced along two distinct paths, those of the so-called direct and indirect measurements. Historically, the latter preceded the former by about a decade, during which time the quality of single crystals was greatly improved and techniques were developed for observing individual dislocations.

Indirect experiments (which employ macroscopic measurements only) invariably require a dislocation model for the interpretation of measurements, and herein lies the disadvantage of the method, for each model employs presuppositions which can only be affirmed by microscopic observations. Of course, no such restraints are imposed on direct measurements, but the experimental techniques here are generally much more sophisticated and difficult to realize.

As far as copper is concerned, mobility studies have been made by both methods [1-5] and there is general agreement only on the order of magnitude of dislocation damping at room temperature. In this thesis, the results of further direct mobility measurements in copper are presented. The work comprised a study of the interaction of individual dislocations with the crystal lattice.

The basic testing apparatus was a torsion machine developed by Pope, et al. [6] and used successfully by them for mobility measurements in zinc [7] and later by Gorman, et al. [8] for work in aluminum. The experimental procedure used here follows essentially their original work.

II. EXPERIMENTAL TECHNIQUES

In this section, the techniques used for obtaining the dislocation velocity-shear stress measurements are discussed. Details which have been adequately described elsewhere are referenced, and the interested reader is referred to them. The experimental procedure can be outlined as follows:

1. A copper single crystal is electrolytically machined into a right circular cylinder with the cylindrical axis in the [111] direction.
2. One end surface is scratched with an $A\ell_2O_3$ whisker to produce dislocations on slip planes parallel to the end surface and about 1 micron below it.
3. The positions of these dislocations are determined from Berg-Barrett x-ray micrographs.
4. The scratched surface of the test crystal is bonded to the torsion apparatus, whereupon a torsional stress pulse is applied to the crystal.
5. The positions of displaced dislocations are established from Berg-Barrett x-ray micrographs.

Test Specimens

Copper single crystals with an orientation near the [111] pole were grown from 99.999 percent pure material by a modified Bridgman technique, similar to that developed by Young and Savage [9]. The parent crystals were acid-sliced perpendicular to the growth direction to obtain cylinders 1 cm long and 2.5 cm in diameter. Each cylinder was then electrolytically machined to provide a single circular test specimen 1.33 cm in diameter, about 0.9 cm long, and with a cylindrical axis within 0.25° of the [111] pole (Figure 1).

The test crystals were annealed for 1 to 7 days at 1040°C in a purified argon atmosphere of 1 psig, and the end surfaces were then lightly electropolished to remove traces of evaporation pits.

Etching the (111) end surfaces of annealed crystals with Livingston's etch [10] revealed between 10^3 to 10^5 dislocation intersections per cm^2. In addition, the crystals were generally free from substructure.

One end surface of each crystal was scratched with an $A\ell_2O_3$ whisker parallel to the three $\langle 110 \rangle$ directions in that surface (Figure 1). The scratching apparatus is well described by Pope [11]. The character of the dislocations produced by the scratching procedure is discussed later.

The Berg-Barrett X-Ray Diffraction Technique

Dislocations on (111) planes less than 2 microns from an end surface of a test specimen were observed by the Berg-Barrett technique, as described by Turner, et al. [12]. Figure 2 is a schematic view of the x-ray apparatus. Characteristic Co radiation diffracted from a set of $\{220\}$ planes provided an image of the near surface of the test crystal on a high-resolution x-ray plate. A pure iron filter, 0.0013 cm thick, absorbed fluorescent radiation. Dislocation Burgers vectors were identified by noting that when the reciprocal lattice vector of the set of diffracting planes was perpendicular to the

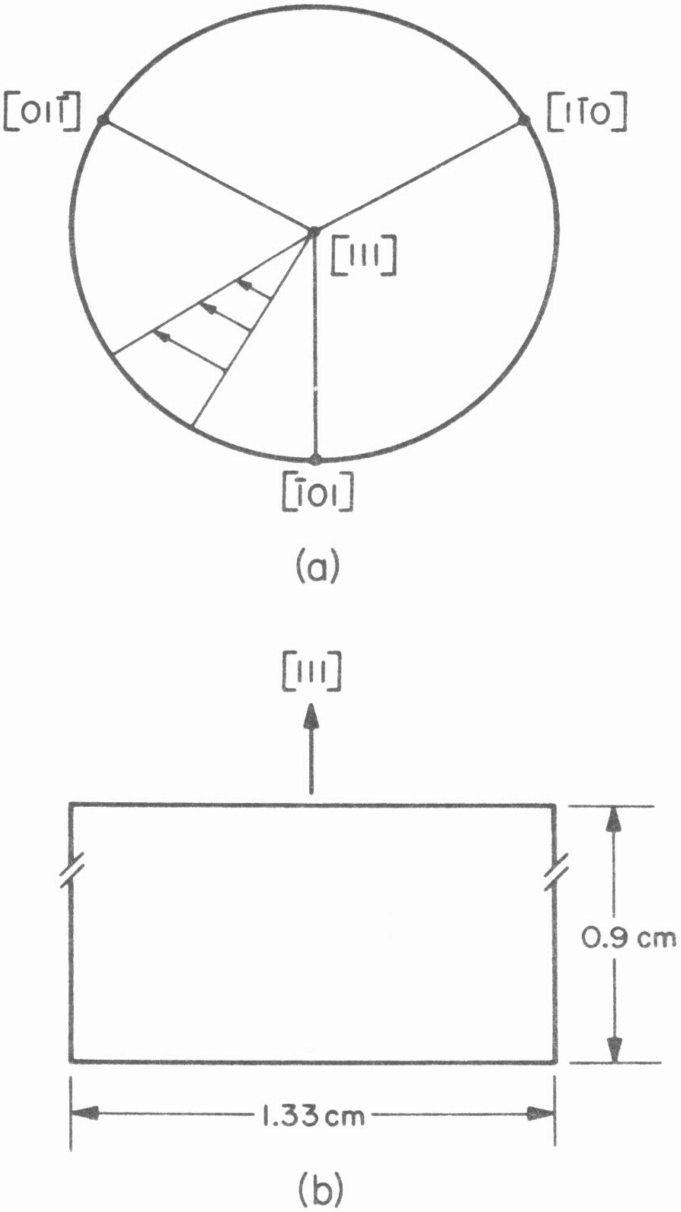

Figure 1. Dimensions and Orientation of Test Crystals. Scratches and Direction of Torsional Stress are Shown in (a).

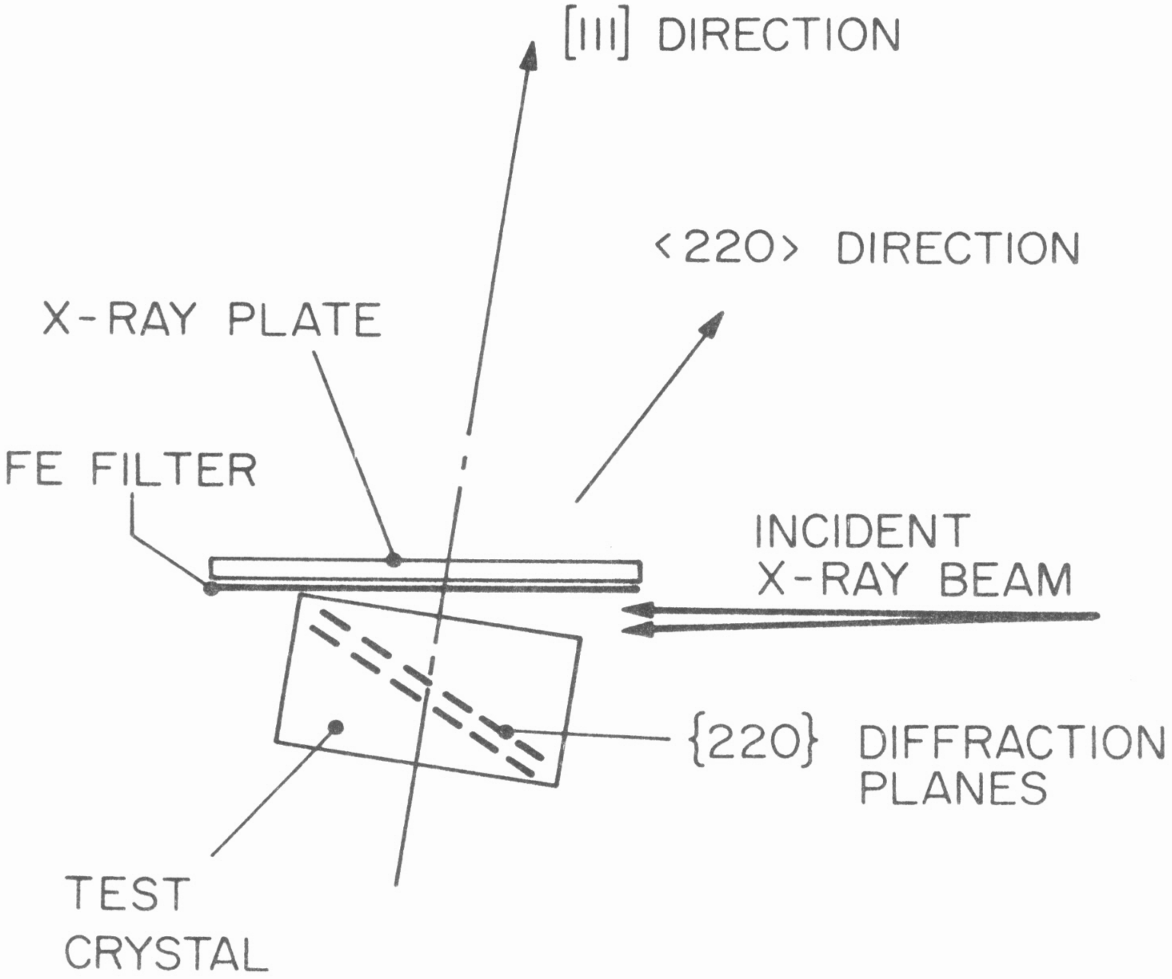

Figure 2. Schematic Diagram of Berg-Barrett Technique.

Burgers vector of a dislocation, the image of that dislocation was nearly extinct. Hence, by obtaining diffraction micrographs from any two of the three available sets of {220} planes, all Burgers vectors in (111) planes could be identified.

The Character of the Selectively-Introduced Dislocations

A typical scratch in a ⟨110⟩ direction produced dislocations on (111) planes with Burgers vectors in either of the two remaining ⟨110⟩ directions (Figure 3a). In addition, dislocations were created on the three {111} cross slip planes (Figure 3b). Etch pits formed where the ends of dislocations on the primary (111) planes cross-slipped to the free surface of the crystal. Dislocations on the primary (111) planes were commonly 0.01 to 0.02 cm in length.

The Torsional Apparatus and Torsion Test

The torsion machine developed by Pope, et al. [6] was slightly modified to accommodate copper test specimens. Steel torsion rods, 1.27 cm in diameter, were used in place of the usual titanium rods. The taper joint assembly below the exploding aluminum foil was replaced by a single steel rod bonded with epoxy to a copper rod. The copper rod was acoustically matched to the steel for elastic torsional waves. Semiconductor strain gages were attached to the copper rod 1.9 cm from its lower end, as shown schematically in Figure 4.

The test specimen, with a cylindrical diameter identical to that of the gage bar, was mounted as shown in Figure 4. A copper extension rod was used in the earlier tests to afford longer stress pulse times, but it proved superfluous and its use was discontinued.

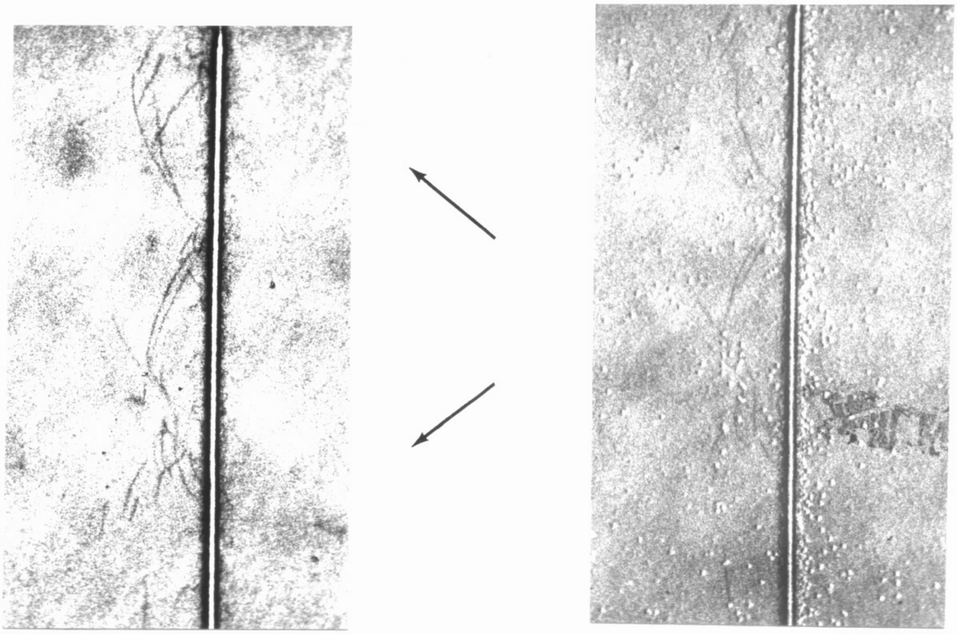

(a) (b)

Figure 3. Typical Scratch Segment Before Testing. (a) Dislocations on Primary Slip Planes with Burgers Vectors $\underline{b}_1$ and $\underline{b}_2$, (b) the Same Area as in (a) but Etched to Reveal Forest Dislocations. Magnification 100X.

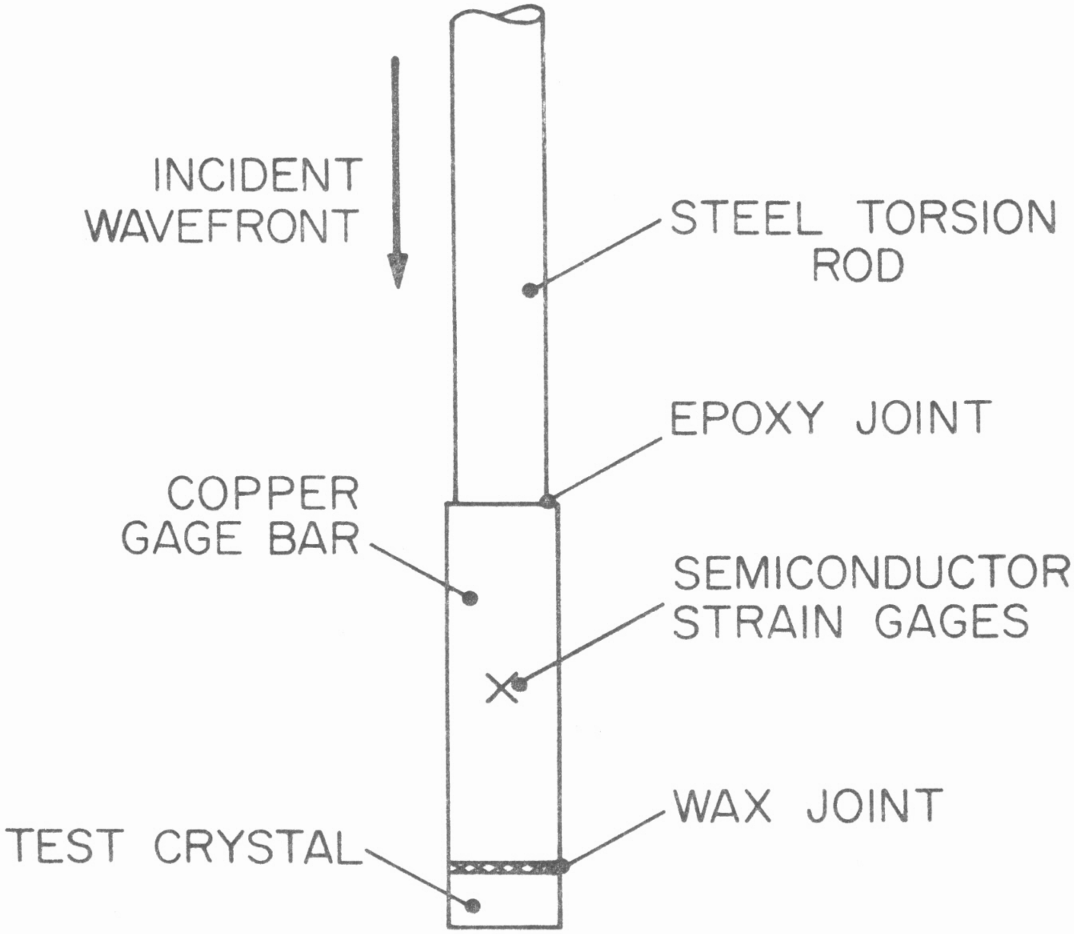

Figure 4. Schematic Diagram of Lower End of Torsion Machine.

The test procedure essentially duplicated that employed by Gorman [13], although the range of his test temperatures was slightly narrower. The bonding agents are listed in Table 1.

TABLE 1. Agents Used to Bond the Test Crystals to the Torsion Machine

Test Temperature (^{o}K)	Bonding Agent	Volumetric Ratio
373	commercial sugar	-
296	quartz-type wax	-
173	glycerine-ethanol	3:2
123	glycerine-ethanol	1:5
83	isopentane-methylcyclohexane	3:1
74	isopentane-methylcyclohexane	10:1
66	isopentane-3-methylpentane	10:1

Two or more tests were made at each temperature. The time between scratching a crystal and torsion testing never exceeded 48 hours. A delay of more than four days produced a measurable decrease in dislocation mobility.

III. EXPERIMENTAL RESULTS

Torsional Stresses in the Test Crystal and the Resolved Shear Stress on Dislocations

The oscilloscope trace of the strain gage output (torque record) for a typical torsion test is found in Figure 5a. In this case, the test crystal is 0.9 cm long and the thickness of the bonding agent (quartz-type sticky wax) is 0.003 cm. While the strain gages provide only a record of the torque in the copper gage bar, it is possible to extrapolate the results to the surface of the copper crystal with knowledge of the elastic properties of the bonding agent and the response of the copper specimen to an incident torsional wave. The former can be well-defined experimentally, but less can be inferred about the behavior of the test crystal. One should refer to Appendices A and B for discussion of these points. The torque record at the test crystal surface is plotted in Figure 5b.

The shear stress on the (111) surface of the test crystal at time t at a radius r from the cylindrical axis of the crystal is:

$$\tau(r,t) = \frac{M(t)r}{I} \qquad (3.1)$$

where M(t) is the torque at the surface at time t, and I is the polar moment of inertia of the crystal.

Torsional stresses exert glide forces on dislocations lying on the cross-slip $\{111\}$ planes as well as those of the primary (111) system. The resolved shear stress on a dislocation on a primary slip plane (Figure 3a) is:

$$\tau_r(r,t) = 0.866\,\tau(r,t) = \frac{0.866}{I}\,M(t)r \qquad (3.2)$$

near its originating scratch, while the resolved shear stress on a dis-

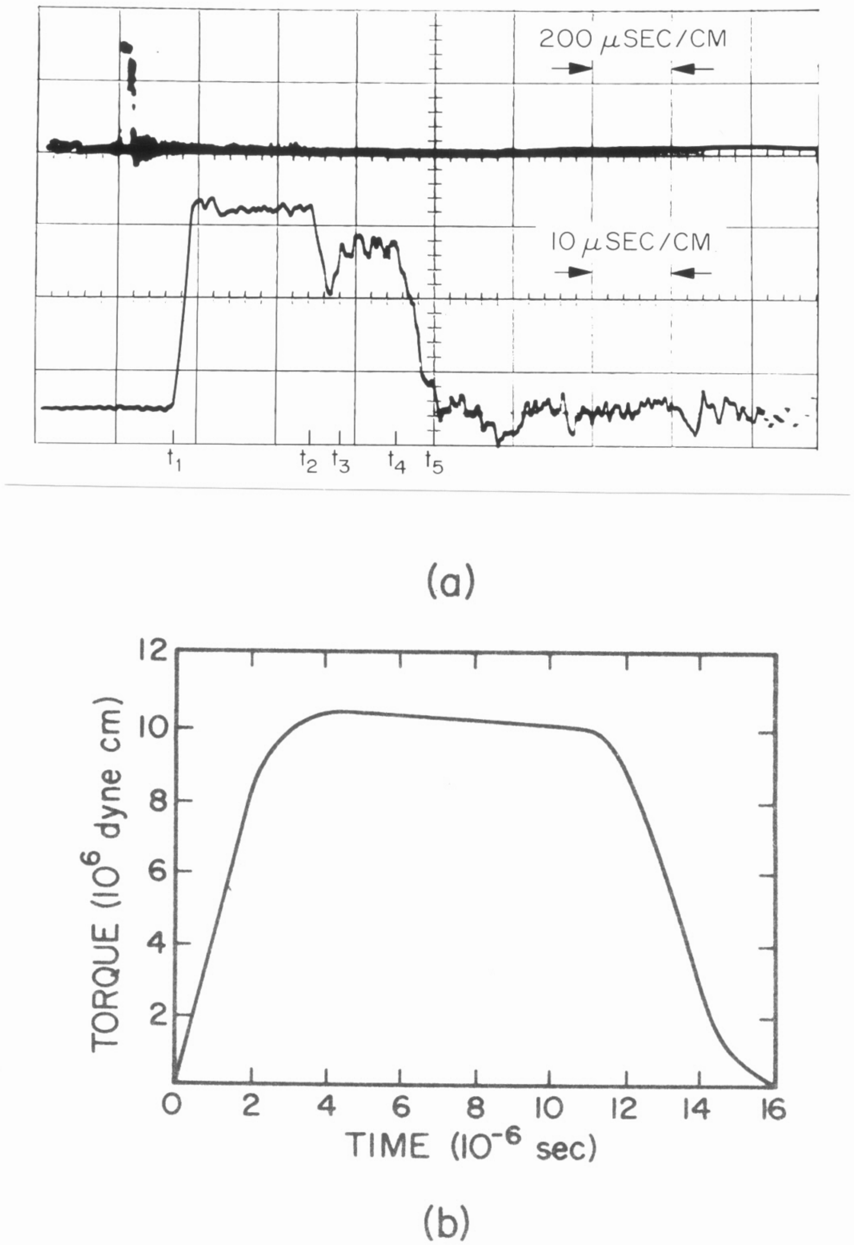

Figure 5. Typical Torque vs. Time Record for Torsion Test. (a) at Strain Gages, (b) Calculated Pulse at Test Crystal Surface.

location of a cross-slip system (Figure 3b) is $\leq \frac{1}{3}\tau_r(r, t)$, depending on the orientation of its Burgers vector.

Dislocation Displacements and the Measurement of Dislocation Mobility

Figures 6a and 6b display the same scratched area of a test crystal preceding and following the torsion test. The region has been etched in Figure 6c to delineate the intersection of forest dislocations with the primary glide system. Etch pits indicate where ends of dislocations on the primary glide planes have cross-slipped to the surface. These cross-slipped segments have obviously constrained the main body of the dislocation to glide in a direction parallel to its Burgers vector when the torsion stress was applied.

The displacements of the farthest moving dislocations lying in the edge orientation after testing were measured as a function of the radius r. These results are cataloged in Figure 7. Displacement measurements are given only for those tests which provided data over a wide range of radius. With the aid of Figure 7, it is possible to write:

$$d(r) = Kr^n \tag{3.3}$$

where $d(r)$ is the maximum dislocation displacement at radius r, and K and n are experimentally determined. If $v(r,t)$ is the dislocation velocity at radius r at time t, then:

$$\int_0^T v(r,t)dt = Kr^n \tag{3.4}$$

where T is the stress pulse time. The relation between dislocation velocity and shear stress is postulated to be:

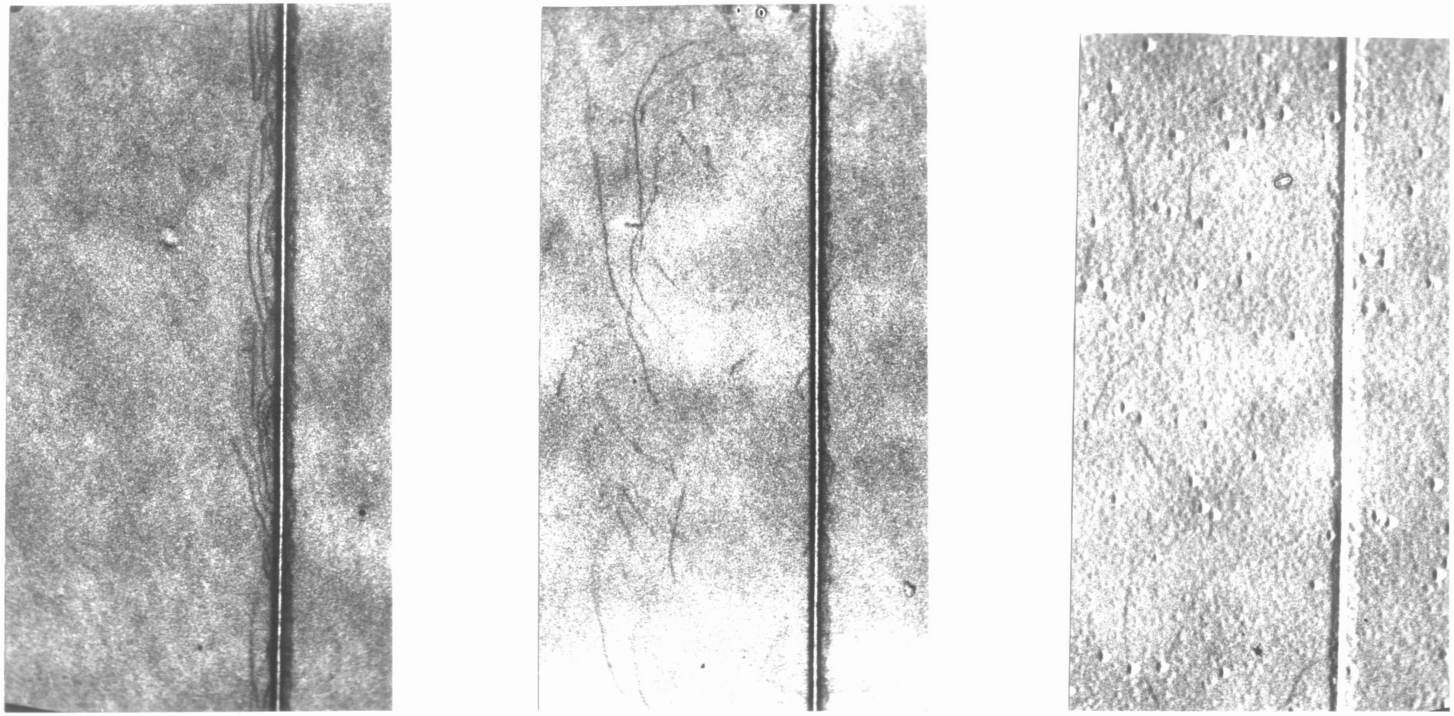

(a) (b) (c)

Figure 6. Typical Scratch Segment. (a) Before Torsion Testing, (b) After Load Application, (c) Same as (b) but Surface Etched to Reveal Forest Dislocations. Magnification 100X.

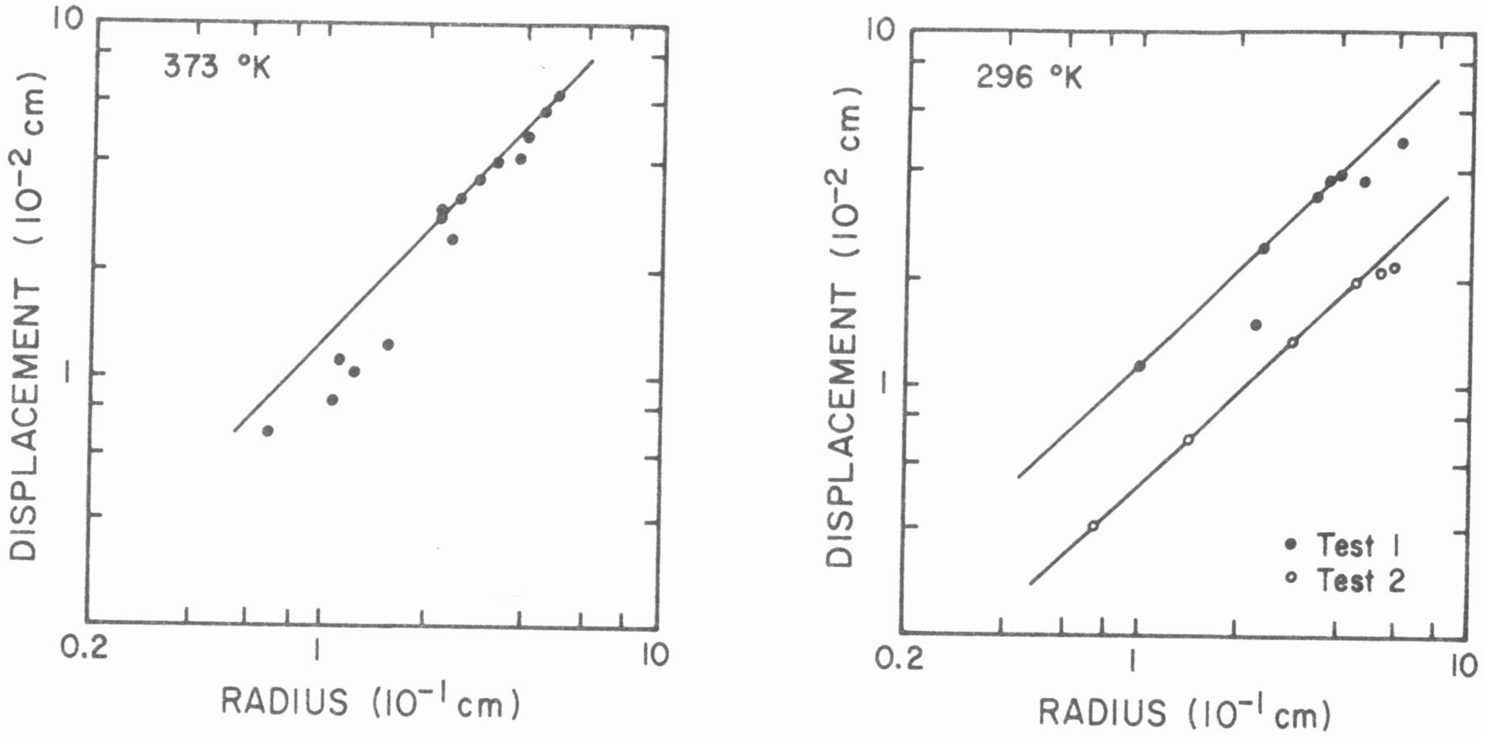

Figure 7. Dislocation Displacement as a Function of Distance r from the Cylindrical Axis of the Test Crystal (for Two Temperatures).

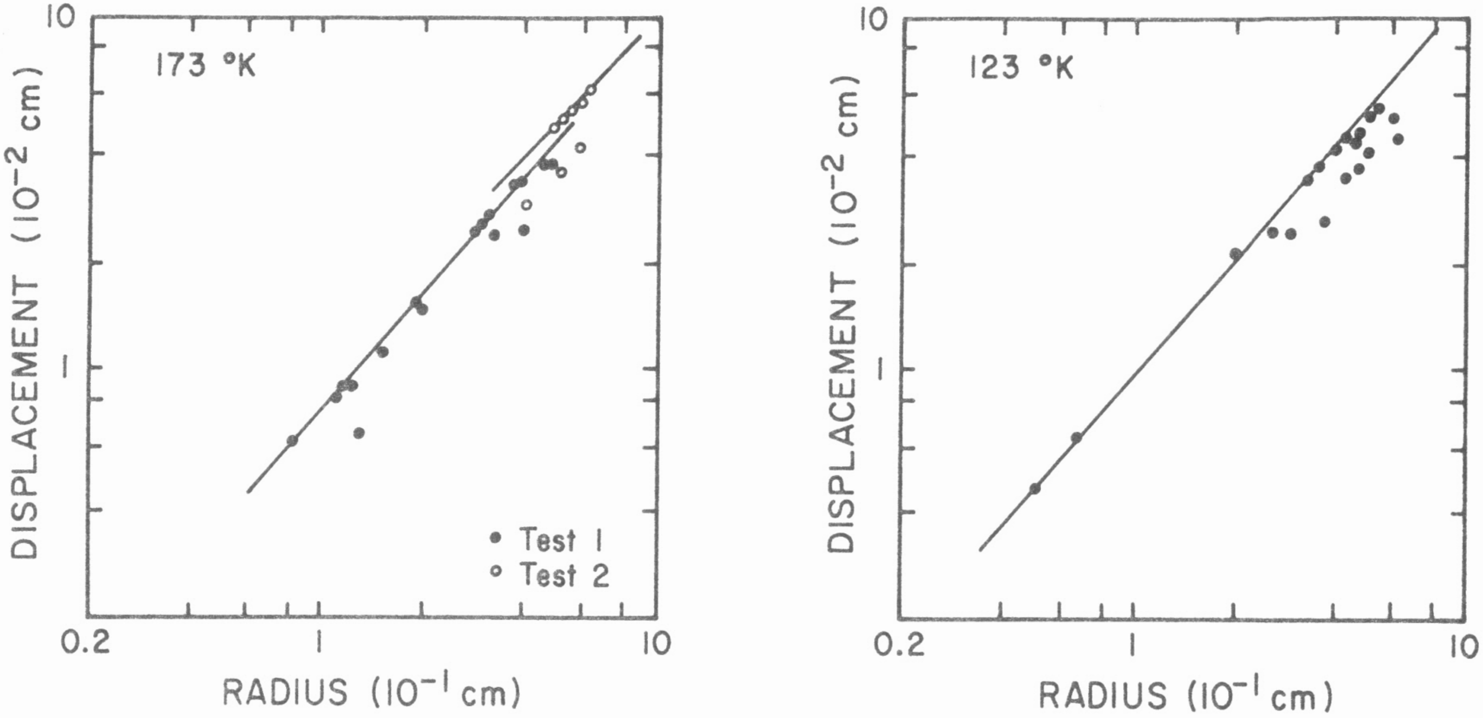

Figure 7. Dislocation Displacement as a Function of Distance r from the Cylindrical Axis of the Test Crystal (for Two Temperatures).
(continued)

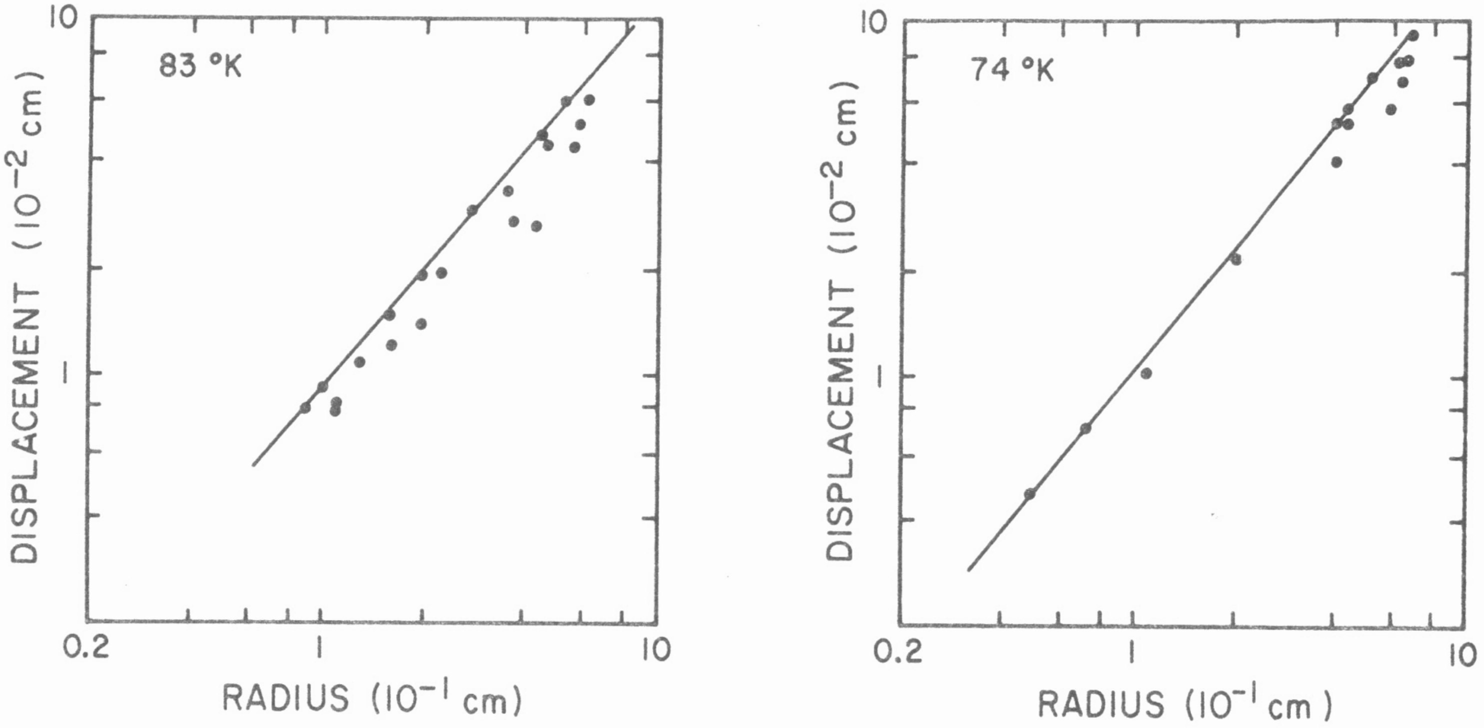

Figure 7. Dislocation Displacement as a Function of Distance r from the Cylindrical Axis of the Test Crystal (for Two Temperatures).
(continued)

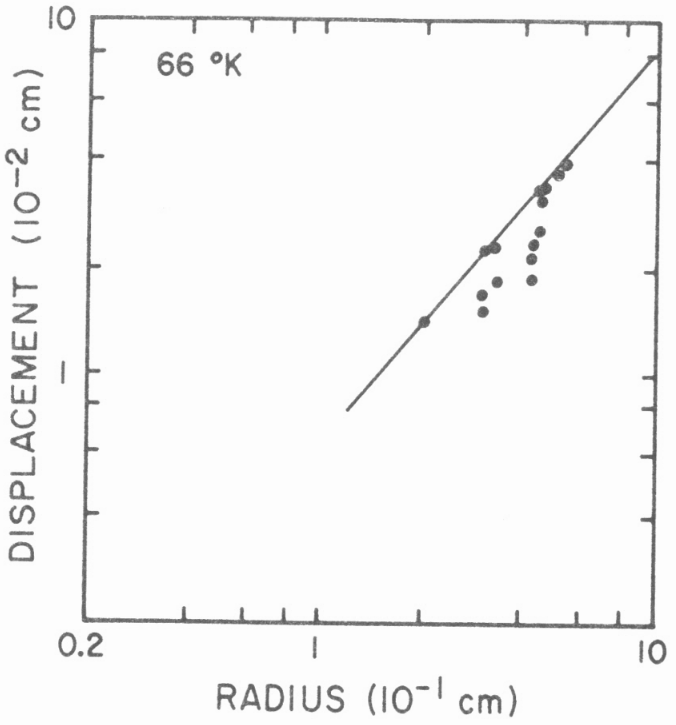

Figure 7. Dislocation Displacement as a Function of Distance r from the Cylindrical Axis of the Test Crystal.

(continued)

$$v(r,t) = v_o \left(\frac{\tau_r(r,t)}{\tau_o} \right)^m \qquad (3.5)$$

where τ_o and m are functions of temperature and v_o is chosen such that v(r, t) equals 2000 cm/sec when $\tau_r(r,t)$ equals τ_o. Then from equation (3. 2):

$$v(r,t) = v_o \left(\frac{0.866\ M(t)}{I\tau_o} \right)^m r^m \quad . \qquad (3.6)$$

Substitution of v(r, t) into equation (3. 4) gives:

$$m = n$$

$$\frac{1}{\tau_o} = \left(\frac{I}{0.866} \right) \left(\frac{K}{v_o \int_0^T M^n(t) dt} \right)^{\frac{1}{n}} \quad . \qquad (3.7)$$

Hence, n is a function of temperature only, while K depends on temperature and the magnitude and duration of the stress pulse. With reference to equation (3. 3) and Figure 7, it is recognized that n is given by the slope of the "best-fit" straight line through the experimental points, while K is determined from the straight line intercepts. τ_o is found from equation (3. 7) upon integration of the torque function $M^n(t)$ (an approximate method of integration is described in Appendix C). The values of n and τ_o are presented in Table II, and the velocity-stress relation is plotted in Figure 8.

The Dislocation Damping Coefficient

If dislocation velocity is directly proportional to the resolved shear stress, it is possible to write:

$$Bv = \tau_r b \quad , \qquad (3.8)$$

where B is the damping coefficient and b is the magnitude of the

TABLE II. Experimentally Determined Values of the Mobility Coefficient, n, and the Resolved Shear Stress, τ_o, Required to Maintain a Dislocation Velocity of 2000 cm/sec.

Temperature °K	Mobility Coefficient, n	τ_o 10^6 dynes cm^2
373	1.00	13.0
296	0.88	16.3
173	1.00	9.5
123	1.03	5.8
83	1.12	4.0
74	1.14	3.6
66	1.10	3.3

dislocation Burgers vector. With a presupposed mobility coefficient equal to 1, the data of Figure 7 may be interpreted by drawing "best-fit" lines of unit slope through the experimental points. Then a comparison of equations (3.7) and (3.8) provides:

$$B = \frac{0.866\,b}{KI} \int_0^T M(t)dt \quad . \tag{3.9}$$

The linearized results are shown in Table III and Figure 9.

TABLE III. Values of the Dislocation Damping Coefficient B, and τ_o, Found by Assuming a Mobility Coefficient Equal to 1.

Temperature °K	Damping Coefficient, B 10^{-4} dynes sec/cm^2	τ_o 10^6 dynes/cm^2
373	1.67	13.0
296	1.70	13.4
173	1.20	9.5
123	0.73	5.7
83	0.60	4.7
74	0.47	3.7
66	0.36	2.8

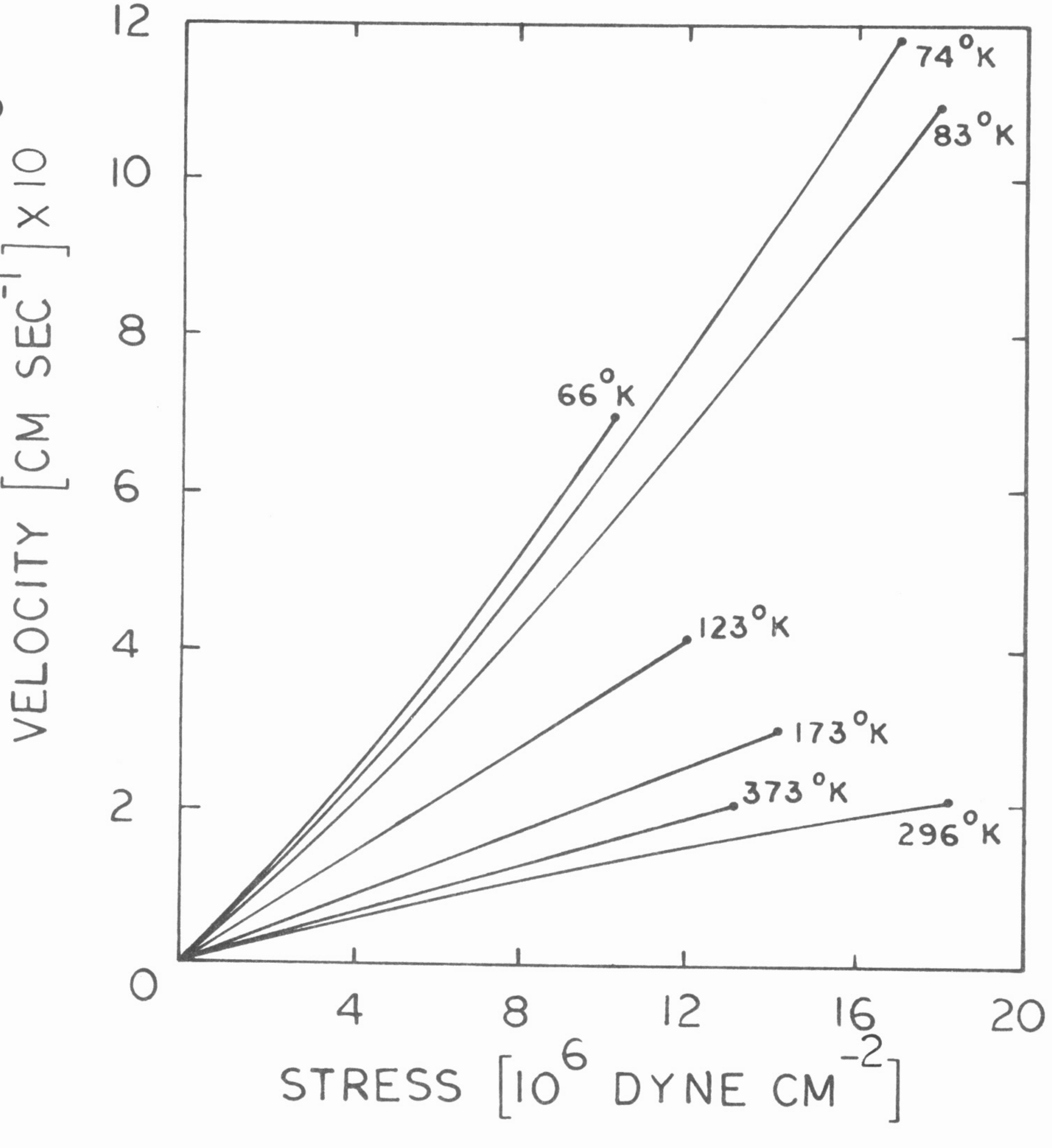

Figure 8. Dislocation Velocity as a Function of Resolved Shear Stress.

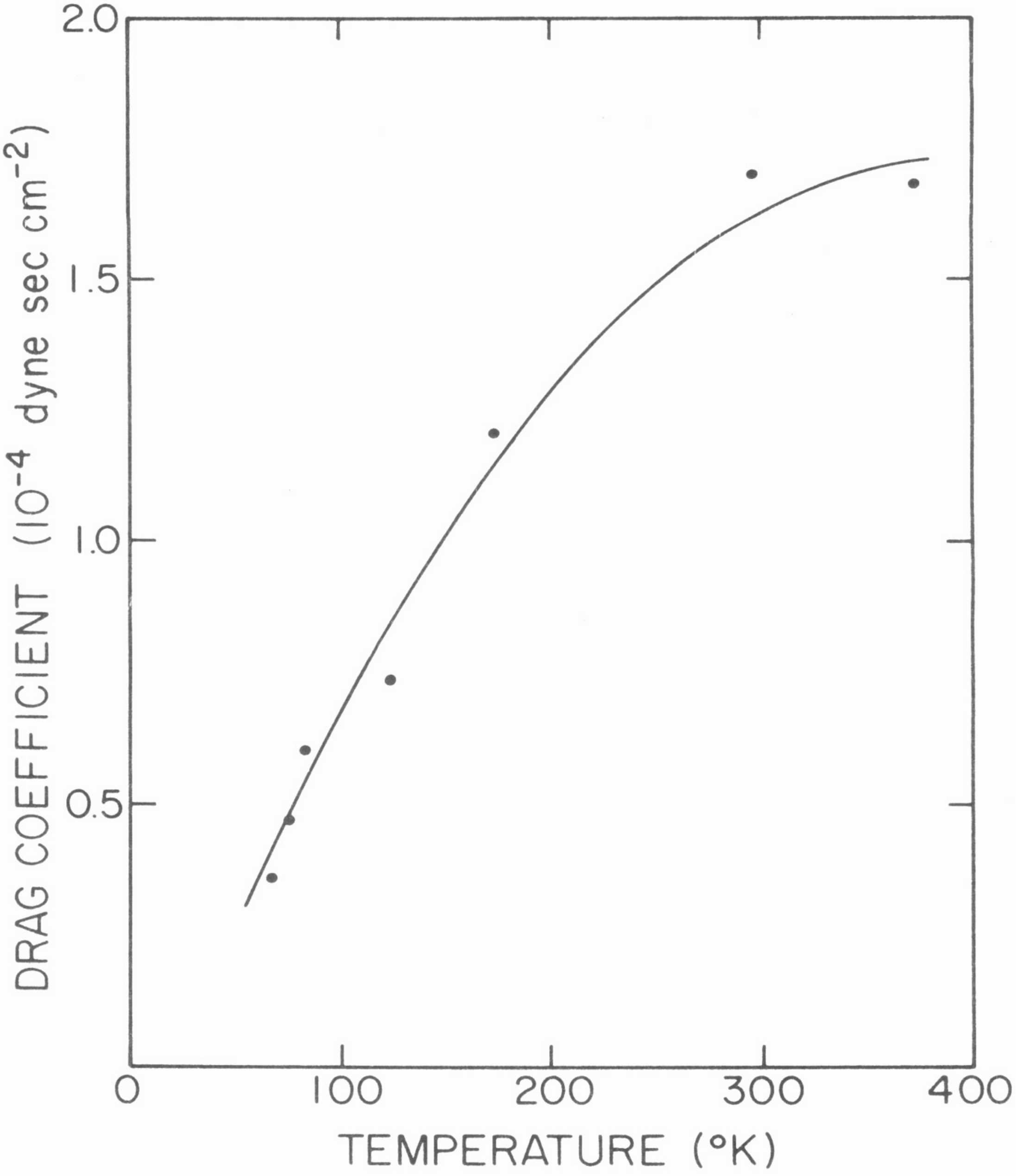

Figure **9.** Dislocation Damping Coefficient for Edge Dislocations in Copper Single Crystals as a Function of Temperature (from Linearized Measurements).

IV. DISCUSSION OF RESULTS

Several points must be considered in the interpretation of the experimental results. In light of the uncertainty in the actual stress state in the crystal (Appendix B), one may question the validity of the observed temperature dependence of the mobility coefficient. Use of equation (3.5) implies that dislocation velocity is in phase with the resolved shear stress, that is, dislocation acceleration times are supposedly negligible in the velocity region considered. Secondly, it is recognized that a dislocation on a primary slip plane glides with its ends on the appropriate cross-slip planes for which the resolved shear stress is considerably reduced. Third, with forest dislocation densities as high as 10^5 etch pits/cm^2, and dislocation displacements of nearly 0.1 cm in some cases, intersection mechanisms cannot be neglected. Finally, it would be desirable to reconcile the present results with previously published work.

Effect of the Uncertainty in the Stress State on the Validity of the Mobility Coefficient

In Appendix B, it was found that the elastic inhomogeneity of the test crystal causes an increase of the tangential shear stress with respect to the pure torsional value for the inner region of the crystal and produces the opposite effect near the outer boundary [equation (B-29)]. The net effect is to underestimate the value of the mobility number. However, one must also consider possible radial shear stresses on the crystal surface required to establish a state of equilibrium. In the limit these could be as large as the deviation of the tangential shear stresses from their pure torsion values. Their effect on dislocation mobility will be different for different Burgers vectors (Figure 3), but must be small relative to the changes in the tangential shear stresses because their resolving factor on the dislocations is 0.5 rather than 0.866.

In conclusion, one can safely assume that the temperature dependence of the mobility coefficient observed experimentally is indeed a real effect and is somewhat underemphasized by the state of stress in the crystal.

Dislocation Acceleration Time

Gorman [13] has discussed non-relativistic acceleration times for a straight dislocation using a mobility coefficient equal to 1. He found an acceleration time constant for aluminum equal to about 10^{-11} seconds. A similar result holds for copper, and it can safely be assumed that dislocation velocity is in phase with applied stress for the velocity range and mobility coefficients found experimentally.

Breakaway of a Dislocation from a Scratch and Its Motion on a Primary (111) Glide Plane

X-ray micrographs revealed that screw components of dislocations on the primary glide system cross-slipped quite readily to the free surface. With the aid of anisotropic elasticity, the free surface attractive stress on the cross-slip plane of a screw dislocation 1 micron below the free surface was estimated to be about 10^7 dynes/cm^2. Since dislocations in copper are extremely mobile at this stress, it is recognized quite readily that any dislocation which assumes a screw orientation will rapidly cross-slip to the free surface. Figure 6 suggests that the primary glide dislocation semi-loops did not expand when motion was induced by the torsional stresses, but rather remained of similar length. This is easily understood if it is assumed that the semi-loops increased in radius until both ends assumed screw configurations, whereupon cross-slip occurred and the dislocations were free to glide through the lattice, with their ends extending to the free surface.

Figure 10 is a schematic representation of an edge dislocation BC on a primary slip plane gliding with velocity v through the crystal lattice. Crystal geometry requires that the applied torsional stress, resolved on the cross-slip plane, act on the segment CD in the direction of motion, while in the opposite direction on AB.

Each of AB and CD constitutes a dragging force on the edge dislocation. In Appendix D the magnitude of these forces is discussed, and it is shown how they can lead to overestimation of the lattice friction force. The overestimation turns out to be negligible for edge dislocations greater than 0.01 cm in length.

Intersection of the Dislocation Forest by Dislocations on the Primary (111) Glide Planes

Maximum dislocation displacements on the primary slip system were about 0.1 cm. The motion of dislocations on other slip systems was considerably less because of their much smaller resolved shear stresses. This implies that the forest dislocations produced in the scratching process (Figure 3b) remained near the scratches during the torsion test. This, of course, is verified in Figure 6c. However, if a dislocation forest density of 10^5 intersections/cm^2 is considered, then a dislocation 0.01 cm in length

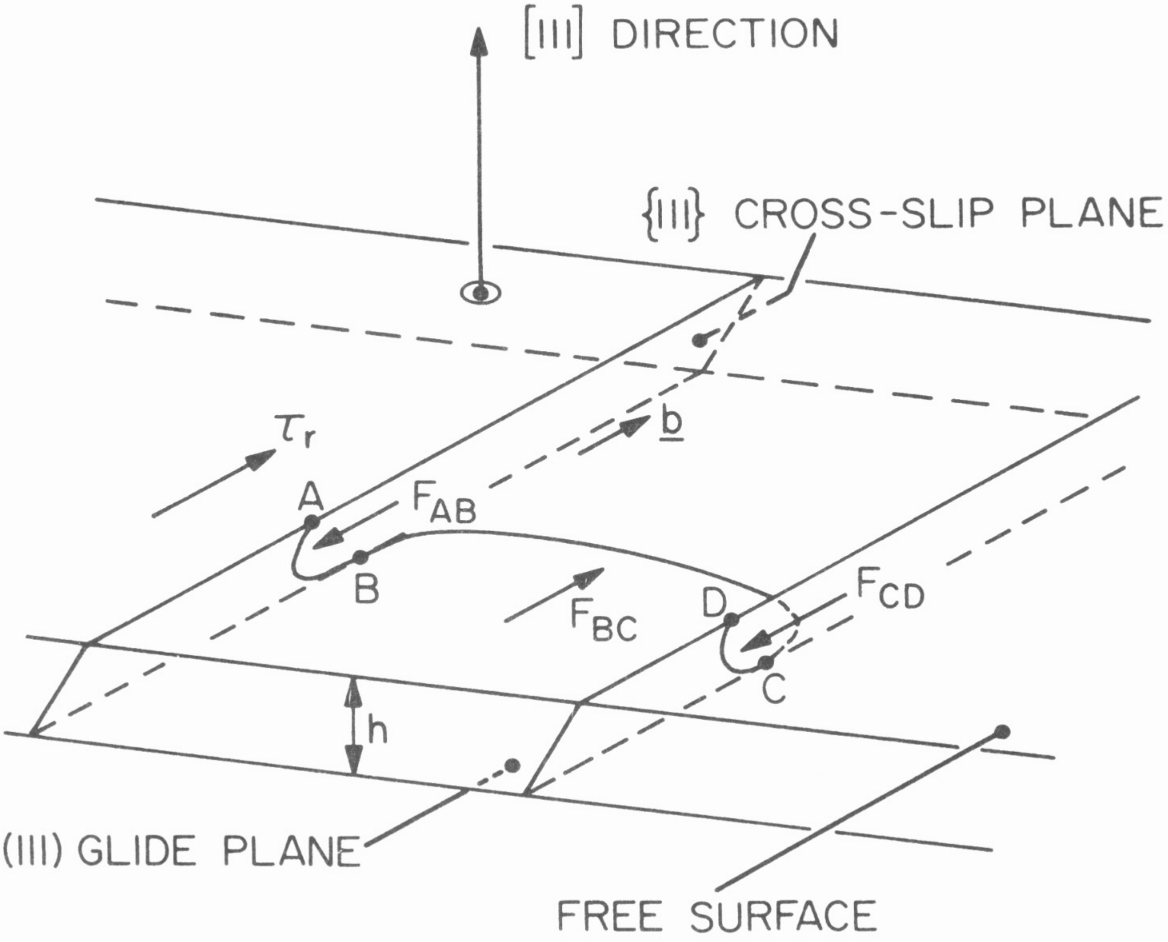

$$F_{AB} = \frac{1}{3}\ \tau_r b + Bv_n$$

$$F_{BC} = \tau_r b - Bv_n$$

$$F_{CD} = -\frac{1}{3}\ \tau_r b + Bv_n$$

Figure 10. Schematic Representation of a Dislocation Gliding on a Primary Slip Plane Under the Influence of Torsional Stresses. F_{AB}, F_{BC}, and F_{CD} are the Normal Forces per Unit Length Acting on the Three Segments of the Dislocation. $\underline{b}$ is the Dislocation Burgers Vector, τ_r is the Resolved Shear Stress on the Segment BC, and h is the Distance from the Primary Slip Plane to the Free Surface.

traveling 0.1 cm on a primary (111) plane experiences, on the average, 100 intersections with the grown-in forest. The number of intersections is decreased by one order of magnitude for each tenfold decrease in forest density. Quite obviously, the strength of the intersection mechanism depends on the length of the mobile dislocation, the distance it moves, the density of forest dislocations, and the type of dislocation interactions.

The experimental techniques presently available can be employed to estimate rather closely the number of forest intersections suffered by each mobile dislocation (Figure 6c), but generally they were not used for this purpose. No correlation is available, from the results of this experiment, between the number of dislocation intersections and dislocation mobility. Instead, Saada's calculation of the stresses required to overcome attractive and repulsive interactions [14] is used. For a randomly distributed forest, Saada estimated that this stress, τ, is given by:

$$\tau = \frac{\mu_o b}{\alpha \ell} , \qquad (4.1)$$

where α is 2.5 for attractive interactions and 10 for repulsive interactions, μ_o is the appropriate isotropic shear modulus, b is the magnitude of the dislocation Burgers vector, and ℓ is the distance between forest trees. In Table 4 are found the largest possible back stress (attractive interactions) in copper for forest densities of 10^3, 10^4, 10^5, and 10^6 intersections/cm^2. All of the dislocation displacement measurements in Figure 7 were from dislocations with resolved shear stresses between the limits of 10^6 and about 1.7×10^7 dynes/cm^2. Hence, according to Saada's calculation, back stresses may be sig-

TABLE IV. Back stress on a Mobile Dislocation on a Primary (111) Slip Plane [from equation (4. 1)].

Back Stress, dynes/cm^2	Forest Dislocation Density, intersections/cm^2
2.3×10^5	10^3
7.0×10^5	10^4
2.3×10^6	10^5
7.0×10^6	10^6

nificant in those regions of the test crystals where forest densities exceed about 10^4 intersections/cm^2. These results, then, predict scatter in the mobility behavior between regions with different forest densities. In the test crystals used, there were an adequate number of areas where dislocation motion on a primary (111) plane was unaffected by the dislocation forest. This, of course, provides justification for choosing "best-fit" curves through the points of greatest velocity in Figure 7.

Comparison of Results with Earlier Experiments

Early estimates of the lattice friction force in pure copper single cyrstals were deduced from internal friction measurements. These measurements were interpreted on the basis of the string model of a vibrating dislocation, the so-called Granato-Lücke theory [15]. (Reference 16, pp. 498-502 gives a clear mathematical description of the model.) In the simple model, the crystal is assumed to contain a network of dislocations, pinned by impurities at various points and by dislocations at network lengths. The model permits the consideration of different distributions of impurities. Each vibrating dislocation segment obeys the differential equation:

$$m \frac{\partial^2 y}{\partial t^2} + B \frac{\partial y}{\partial t} - C \frac{\partial^2 y}{\partial x^2} = F(t) \ , \tag{4. 2}$$

where y is the dislocation displacement at a point x along the dislocation line, F(t) is the forcing function at time t, m is the dislocation effective mass, B is the damping coefficient, and C is the dislocation line tension.

A harmonic stress, $\tau(t) = F(t)/b$, with frequency ω, is impressed upon the crystal. The solution of equation (4. 2) then provides the energy loss per cycle of stress, or, in normalized form, the logarithmic decrement Δ. If breakaway from pinning points is excluded, then:

$$\Delta = \alpha \mu_o \delta \left[\frac{\omega T}{1 + (\omega T)^2} \right] \ , \tag{4. 3}$$

where α is an orientation factor resolving the harmonic stress onto the various slip systems, and μ_o is the static isotropic shear modulus. δ and T are given by:

$$\begin{aligned} \delta &= \frac{b^2 L}{\pi^3} \left(\frac{\ell^2}{C} \right) \ , \\ T &= \frac{B}{\pi^2} \left(\frac{\ell^2}{C} \right) \ . \end{aligned} \tag{4. 4}$$

b is the magnitude of the dislocation Burgers vector, ℓ is the average loop length, and L is the total length of mobile dislocation line.

Several weaknesses of the model are recognized immediately. Equation (4. 2) considers only a mobility coefficient of 1, and no account is taken of the difference in line tension or damping coefficient between dislocations of unlike character. In addition, the magnitude of the impressed stress in the megacycle frequency range limits dislocation velocities to less than 10 cm/sec.

The dislocation elastic strain also gives rise to a decrease in the effective shear modulus, but measurements of the decrement are generally more reliable than those of the modulus decrease. Using decrement measurements alone, the problem of obtaining the magnitude and temperature dependence of the damping coefficient may be approached in three ways.

The first two methods require the measurement of the decrement as a function of frequency at every temperature in the range under consideration. The maximum decrement, Δ_{max}, is found when:

$$\omega T = 1 \ , \tag{4.5}$$

or

$$\Delta_{max} = \frac{\alpha \mu_o \delta}{2} \ . \tag{4.6}$$

Combining equations (4.5) and (4.6) with equation (4.4) gives:

$$\frac{B}{L} = \frac{\alpha \mu_o b^2 2\pi}{\omega \Delta_{max}} . \tag{4.7}$$

With a suitable assumption for the total length of mobile dislocations, B is determined as a function of temperature.

Alternatively, one may appeal to the asymptotic value of the decrement in the frequency region where $\omega T >> 1$. Then the asymptotic form of equation (4.3) is used, and

$$\Delta \rightarrow \frac{\alpha \mu_o b^2}{\pi \omega} \left(\frac{L}{B}\right) , \tag{4.8}$$

and B may be found as before.

The third approach, on the other hand, necessitates the measurement of the decrement at only one frequency, but as a function of temperature on the same crystal. However, the method requires that δ be temperature-independent, and this is a postulate for which there is little justification. Proceeding in the analysis, one finds that:

$$2\,\Delta_{\max} = \alpha\,\mu_o\,\delta\ , \tag{4.9}$$

where $\Delta_{\max}$ is determined from the temperature dependence of Δ. The variation of T with temperature is found from equation (4.3). Again, ℓ^2/c may be eliminated and B estimated as a function of temperature.

Validation of any of the above simple methods can come only through experimental verification of equations (4.3) or (4.8). Quite obviously, agreement will be best if the majority of mobile dislocations are of the same character and the distance between pinning points is uniform. The weakness of all three approaches is the uncertainty in L.

Alers and Thompson [1] reported the first indirect measurements of the damping coefficient in copper. They used both the first and last of the aforementioned methods to find B. Their experimental measurements were in fair agreement with the predictions of equation (4.3). Interestingly, they found that B decreased by about a factor of 4 between room temperature and 60°K, a result similar to the deductions of our work. They estimated the room temperature value of B to be about 10^{-4} dynes sec/cm^2 using the first method and 8×10^{-4} dynes sec/cm^2 using the second, less accurate technique.

Stern and Granato [2] refined the simple theory by considering the vibrating dislocations to be of two distinct types, edge and screw, with significantly different line tensions. They postulated that each dislocation type obeyed the Granato-Lücke theory and was pinned with an exponential distribution of loop lengths. The damping coefficient was assumed to be the same for both edge and screw dislocations. On this basis, Stern and Granato successfully predicted the effects of temperature and neutron irradiation on the energy decrement. They concluded that $B \leq 6.5 \times 10^{-4}$ dynes sec/cm^2 at room temperature.

Suzuki, et al. [3] used the asymptotic formula for the decrement [equation (4.8)] to interpret their measurements on two crystals. They found B equal to 2.7×10^{-5} dynes sec/cm^2 for one crystal and 1.2×10^{-5} dynes sec/cm^2 for the second, both at room temperature. It appears that the discrepancy between the two measurements is the result of misapplication of equation (4.8). Apparently the experimental data were all taken near the rather broad maximums of the decrements (Figures 3 and 4 of Reference 3), and thus the asymptotic forms of Δ for both crystals required rather gross extrapolation. Indeed, if one examines from their experimental data the magnitude of the factor $(\alpha \mu_0 b^2)/\pi$, which should not vary from crystal to crystal (provided the crystals have the same orientation with respect to the exciting stresses), values of 0.37 and 0.85 are found for the two crystals. This result would suggest that the simple model is not sufficient to describe their results. The broad Δ vs. ω curves suggest an interpretation on the basis of the more refined model put forward in [2].

Marukawa [4] measured directly dislocation mobility in pure copper at room temperature by applying stress pulses to single crystals in a 4-point bending jig. A similar etching technique was used by Greenman, et al. [5] for measurements in single crystals subjected to torsional stress pulses. While Marukawa's measurements were taken from grown-in dislocations, Greenman, et al. introduced dislocations into the test crystals with a scratching apparatus.

Marukawa found a mobility coefficient of 2. It is difficult to make a realistic appraisal of the lattice damping from his results because the extent of the segregation of impurities and lattice defects to his dislocations and their corresponding effects on dislocation motion are unknown, as is the extent of interaction with other dislocations. Also, Marukawa conducted his tests over a limited range of resolved shear stress (0.5×10^6 to 3×10^6 dynes/cm^2), which makes his determination of the mobility coefficient relatively inaccurate.

Greenman, et al. were burdened by the problem of grown-in dislocations only with reference to their influence on the motion of freshly introduced dislocations. For resolved shear stresses from about 2×10^6 to 2×10^7 dynes/cm^2, Greenman, et al. reported a mobility coefficient of 0.7 at room temperature. They then linearized their measurements by choosing $n = 1$ and determined a damping coefficient equal to 7×10^4 dynes sec/cm^2. It is recalled that Greenman, et al. used average dislocation displacements rather than maximum displacements to obtain their results, and one then realizes that this factor significantly affects the magnitude of B. It must also be remembered that there is uncertainty as to the character of their mobile dislocations, although they were probably near the 30° mixed type.

The results of Greenman, et al. and those presented in this thesis indicate that the mobility coefficient at room temperature is slightly smaller than 1, most probably between the limits of 0.7 and 0.9 for both edge and mixed dislocations. The indirect measurements provide the correct order of magnitude of damping in copper, but of course cannot give a measure of the mobility number. The results of Alers and Thompson are encouraging in view of their prediction of the temperature dependence of B. The results of Stern and Granato and Suzuki, et al. suggest that, in the general case, the complexity of dislocation configurations in the test crystals precludes an interpretation by the simple model.

Summary

The velocity of edge dislocations in pure copper single crystals was measured as a function of resolved shear stress for 7 temperatures from 66°K to 373°K. The range of shear stress was 0 to 1.5×10^7 dynes/cm^2. The maximum dislocation velocity was about 9000 cm/sec at low temperatures.

Experimentally, the mobility coefficient decreased from 1 to about 0.88 when the test temperature was decreased from 373°K to 296°K. Below 296°K the mobility coefficient increased with decreasing temperature to about 1.1 at 66°K.

Several weaknesses in the experimental approach and suggestions for refinement are apparent. The first test crystals were not annealed for sufficient periods. One week's anneal decreased tenfold the etch-pit density on the crystal surface with respect to one day's anneal. In the process, dislocation densities commonly were reduced from between 10^4 and 10^5 to about 10^3 to 10^4 cm^{-2}. Of course, the longer annealing periods played a significant role in reducing interactions with the dislocation forest. Unfortunately, the softer crystals created more severe problems with respect to plastic flow. In an interesting paper, Johnson and Ashby [17] demonstrated that the minimum stress for dislocation multiplication in copper crystals (about 10^6 $dynes/cm^2$) occurs for densities between 10^3 and 10^4 cm^{-2}, so that the better crystals were subject to the worst conditions for significant plastic flow. However, their analysis also shows that the multiplication stress increases quite rapidly for lower dislocation densities. For example, this stress increases to about 10^8 $dynes/cm^2$ for a density of 10^2 cm^{-2}. This stress is above the present capability of our equipment, while the low dislocation density should be easily attainable with our present equipment for crystal growth and preparation. A significant decrease in plastic flow would certainly provide more certainty as to the stress state in the crystal.

Forest dislocations were undoubtedly the main source of scatter in the experimental measurements. The effect of the dislocation configuration on measurement errors was discussed, and was found to be negligible.

The characteristics of dislocation motion were consistent with an interpretation on the basis of damping by thermal phonons. The relevance of the various phonon drag theories to the experimental results presented here is indicated in Appendix E.

APPENDIX A

RISE AND DECAY OF THE TORSIONAL WAVE

In the discussion to follow, and in Appendix B, it is assumed that the steady-state elastic stresses and strains in the isotropic loading rod (gage bar and bonding agent) may deviate from that of pure torsion because of the particular elastic behavior of the (111) axis test crystal. However, in accordance with St. Venant's Principle, one considers that the elastic state decays to the pure torsional case at the height of the strain gages (Figure 4).

With reference to Figure 5a, a description of the torsional wave can be given. At time t_1, the wavefront arrives at the strain gages. Less than 2 microseconds are required to attain the maximum torque. The round-trip travel time of the wave between the strain gages and the bond is (t_2-t_1). The sharp drop at this time represents wave reflection from the soft bonding agent. At time t_3, the wave has built up across the bond to its maximum value. The decreasing height between t_3 and t_4, the so-called steady state region, represents a small dissipation of torque from plastic deformation in the test crystal. The round-trip travel time of the wave in the test crystal is approximately equal to (t_4-t_2), while (t_5-t_4) is the time required for the wave reflected from the free end of the test crystal to decay through the bond. Note that the rise time of the wave has increased from 2 to more than 4 microseconds after two passes through the soft bonding agent.

The torque record of Figure 5a can be constructed mathematically with knowledge of the elastic properties of the bonding agent, the bond thickness, and the acoustic mismatch between the gage bar and test crystal. Conversely, the elastic properties of the bonding agent can be determined from the torque record for a polycrystalline copper cylinder acoustically matching the gage bar, allied with the proper mathematical equations. With knowledge of the elastic properties of the bonding agent and the bond width, the torque at the surface of a test crystal can be found as a function of time for any test. The reader is referred to Appendix B of Reference 13 for a mathematical discussion of the transfer of energy across the bond. The precise calculation of the torque record for the test crystal requires numerical solution by machine techniques. In Figure 5b, such a solution for the torque record of Figure 5a is provided.

APPENDIX B

TORSIONAL STRESSES IN THE TEST CRYSTAL

Because of elastic anisotropy, a pure torsional wave cannot be propagated without dispersion in a $\langle 111 \rangle$ direction in copper. Hence, the torsional stresses and displacements of the incident wave cannot be simultaneously realized at the surface of a test crystal, and some type of wave dispersion must follow.

A second, and as will be apparent, more critical problem is the elastic shear modulus defect due to the presence of grown-in dislocations in the test crystal. Koehler and deWit [18] have treated this effect in detail for fcc crystals. They showed that the shear modulus of copper can be reduced by several percent for small dislocation strains. The effect is much more pronounced for this experiment, as dislocations strains are no longer small. Indeed, using the analysis of [19], a stress less than 1.2×10^6 dynes/cm^2 is required to bow out into the Frank-Read configuration an edge dislocation initially 0.01 cm long.

The shear modulus relating applied stress to dislocation strain decreases by a factor greater than 5 from the low stress to high stress range. One can write:

$$\delta S_e + \delta S_d = \frac{\delta \tau}{\mu_{eff}} \qquad \text{(B-1)}$$

where δS_e is a change in elastic strain, δS_d is a change in dislocation strain, μ_{eff} is the effective shear modulus, and $\delta \tau$ is the corresponding change in applied stress. If μ_o is the perfect crystal shear modulus and μ' is the modulus relating stress to dislocation strain, then:

$$\frac{\delta\tau}{\mu_o} + \frac{\delta\tau}{\mu'} = \frac{\delta\tau}{\mu_{eff}} \quad , \tag{B-2}$$

and the modulus defect $\delta\mu/\mu_o$ is given by:

$$\frac{\mu_o - \mu_{eff}}{\mu_o} = \frac{\mu_o}{\mu' + \mu_o} \quad . \tag{B-3}$$

In the low stress range, say,

$$\delta\mu/\mu_o = 0.04 \; , \tag{B-4}$$

then

$$\mu' = 24\,\mu_o . \tag{B-5}$$

In the high stress range,

$$\mu' \simeq 5\mu_o , \tag{B-6}$$

and

$$\delta\mu/\mu_o \simeq 0.17 \quad . \tag{B-7}$$

Quite obviously, the modulus defect will increase with distance from the cylindrical axis of a crystal.

The torque record (Figure 5a) indicates significant reflection of the incident torsion wave at the crystal surface (time t_2). The acoustic mismatch can be attributed to a combination of the effects discussed above. The modulus defect from dislocation strain, for any test crystal, increases with increasing applied torque. Due to this, the fraction of incident torque reflected must increase for incident waves larger in magnitude. However, one would expect the fraction of the incident torsional wave reflected because of elastic anisotropy to remain independent of the strength of the incident wave if the two effects do not interact strongly. The relative importance of the two effects was determined through two torsion tests with different applied torques on the same crystal. The results are summarized in Table 5.

TABLE 5. Fraction of Incident Torsional Wave Reflected at the Surface of a Test Crystal and Magnitude of the Effective Wave Velocity in the Crystal, for Two Wave Strengths.

Test No.	Maximum Torque (10^6 dyne-cm)	Fraction of Incident Wave Reflected	Effective Wave Velocity 10^5 cm sec^{-1}
1	12.3	0.18	1.65
2	3.7	0.08	1.92

Table 5 implies that the modulus defect is the main source of acoustic mismatch. The effective wave velocity in the test crystal is defined as the velocity with which the main body of the torsional wave traverses the crystal. It is given by the length of the crystal divided by the round-trip travel time ($t_4 - t_2$) in Figure 5a. In accord with the modulus defect, this velocity decreases as torque increases.

It remains to determine the state of stress at the surface of the test crystal, in light of the results above.

The elastic anisotropy of the crystal, when considered alone, does not produce significant reflection of the incident torsional wave at the boundary between the gage bar and crystal. This implies that the moment, about the cylindrical axis, of the shear stresses acting on the crystal surface is equal to the applied torque. However, as mentioned previously, the anisotropy does not permit the realization of both torsional stresses and displacements in the crystal.

There are two limiting cases for the boundary condition on the end surface of the crystal in the steady state:

(a) The isotropic loading rod (gage bar and bonding agent) is assumed to be extremely compliant. Then the stresses on the end surface of the crystal are purely torsional.

(b) The isotropic loading rod is considered to be extremely rigid. Then the displacements on the end surface of the crystal are purely torsional.

Boundary condition (a) is attractive because it provides for stress-free lateral boundaries, while (b) does not. Case (a) is considered in the following.

An orthogonal coordinate system is defined by:

$$x_1 = [11\bar{2}] \; ; \; x_2 = [\bar{1}10] \; ; \; x_3 = [111] \; . \qquad \text{(B-8)}$$

Then the state of torsional stress in the crystal is:

$$\begin{aligned} T_4 &= -\alpha x_1 \\ T_5 &= \alpha x_2 \\ \text{all other } T_i &= 0 \end{aligned} \qquad \text{(B-9)}$$

which satisfies the stress equations of equilibrium and provides stress-free lateral boundaries. α is a number that depends on the total torque.

The matrix of elastic compliances for the coordinate system of equation (B-8) is [20]:

$$\begin{pmatrix} s_{11} & s_{12} & s_{13} & 0 & s_{15} & 0 \\ s_{12} & s_{11} & s_{13} & 0 & -s_{15} & 0 \\ s_{13} & s_{13} & s_{33} & 0 & 0 & 0 \\ 0 & 0 & 0 & s_{44} & 0 & -2s_{15} \\ s_{15} & -s_{15} & 0 & 0 & s_{44} & 0 \\ 0 & 0 & 0 & -2s_{15} & 0 & s_{66} \end{pmatrix}$$

In terms of the three independent compliances (s'_{11}, s'_{12}, s'_{44}) with coordinate axes in the directions of the cubic axes, one finds:

$$
\begin{aligned}
s_{11} &= s'_{11} - \tfrac{1}{2} D \\
s_{33} &= s'_{11} - \tfrac{2}{3} D \\
s_{12} &= s'_{11} + \tfrac{1}{6} D \\
s_{13} &= s'_{12} + \tfrac{1}{3} D \\
s_{44} &= s'_{44} - \tfrac{4}{3} D \\
s_{66} &= s'_{44} + \tfrac{2}{3} D \\
s_{15} &= -\sqrt{2}/3\, D
\end{aligned}
\qquad \text{(B-10)}
$$

where

$$D = s'_{11} - s'_{12} - \tfrac{1}{2} s'_{44} \; . \qquad \text{(B-11)}$$

The elastic strains follow immediately, and these are expressed in terms of the displacement derivatives, $U_{i,j}$.

$$
\begin{aligned}
U_{1,1} &= \alpha s_{15} x_2 \\
U_{2,2} &= -\alpha s_{15} x_2 \\
U_{3,3} &= 0 \\
U_{2,3} + U_{3,2} &= -\alpha s_{44} x_1 \\
U_{1,3} + U_{3,1} &= \alpha s_{44} x_2 \\
U_{1,2} + u_{2,1} &= 2\alpha s_{15} x_1
\end{aligned}
\qquad \text{(B-12)}
$$

The displacements are found by integrating equations (B-12), and, neglecting rigid body motion, they are:

$$\begin{aligned} U_1 &= \{\alpha s_{15} x_1 x_2\} + \alpha s_{44} x_2 x_3 \\ U_2 &= \left\{\frac{\alpha s_{15}(x_1^2 - x_2^2)}{2}\right\} - \alpha s_{44} x_1 x_3 \\ U_3 &= 0 \end{aligned} \tag{B-13}$$

The non-torsion displacements are emphasized by the curly brackets. Of course, this is not the exact solution to the problem posed in the present experiment because the loading rod is not infinitely compliant. One can, however, obtain a measure of the maximum deviation of the stresses from the pure torsion state by considering that the non-torsional displacements are accommodated entirely in the bonding agent. These can be considered to increase from zero, at the gage bar, to the values given in the curly brackets, at the crystal surface. If L is the bond thickness, then the average strains in the bonding agent due to the anisotropic effect are:

$$\begin{aligned} S'_4 &= \frac{\alpha s_{15}(x_1^2 - x_2^2)}{2L} \\ S'_5 &= \frac{\alpha s_{15} x_1 x_2}{L} \end{aligned} \tag{B-14}$$

with accompanying stresses:

$$\begin{aligned} T'_4 &= \frac{\alpha s_{15}\mu(x_1^2 - x_2^2)}{2L} \\ T'_5 &= \frac{\alpha s_{15}\mu x_1 x_2}{L} \end{aligned} \tag{B-15}$$

where μ is the shear modulus of the bonding agent.

In the worst possible case, the torsional stress state will be deformed by the values of T'_4 and T'_5. When compared to the torsional stresses, they are found to be insignificant. Consider:

$$\left|\frac{T'_5}{T_5}\right| = \left|\frac{s_{15}\mu x_1}{L}\right| \quad . \tag{B-16}$$

Hearmon [21] lists the values of the three independent stiffnesses, and for copper:

$$s'_{11} = 14.5 \;;\; s'_{12} = -6.05 \;;\; s'_{44} = 14.6 \tag{B-17}$$

in units of 10^{-13} cm^2/dyne. Then, using equation (B-10):

$$s_{15} = -6.2 \times 10^{-13} \text{ cm}^2/\text{dyne} \quad . \tag{B-18}$$

Customarily, the bonding agent had characteristics close to the following:

$$\begin{aligned} \mu &= 4 \times 10^8 \text{ dynes/cm}^2 \\ L &= 5 \times 10^{-3} \text{ cm} \end{aligned} \tag{B-19}$$

Then the maximum value of $|T'_5/T_5|$ is found from equations (B-16), (B-18), and (B-19) when $x_1 = 0.67$ cm .

$$|T'_5/T_5| < 0.04 \tag{B-20}$$

The elastic inhomogeneity due to the presence of dislocations in the crystal poses a more serious problem than elastic anisotropy. The cylindrical crystal now can be considered as elastically isotropic, but with radially-dependent elastic moduli. Again, one finds the same two limiting conditions on the end boundary as before, but now both satisfy the requirement of a stress-free lateral boundary. In the following, boundary condition (b) is considered. This provides the case for the most severe possible distortion of the stress state.

The coordinate system of equation (B-8) is used, but an isotropic, inhomogeneous shear modulus, $\mu(r)$, is assumed, where r is the distance from the cylindrical axis of the crystal. Then:

$$
\begin{aligned}
U_1 &= -\beta x_2 x_3 \\
U_2 &= \beta x_1 x_3 \\
U_3 &= 0
\end{aligned}
\tag{B-21}
$$

where β is the angle of twist per unit length. The corresponding strains are:

$$
\begin{aligned}
S_4 &= \beta x_1 \\
S_5 &= -\beta x_2
\end{aligned}
\tag{B-22}
$$

and, using Hooke's law, the elastic stresses are:

$$
\begin{aligned}
T''_4 &= \mu(r)\beta x_1 \\
T''_5 &= -\mu(r)\beta x_2
\end{aligned}
\tag{B-23}
$$

To a first approximation, $\mu(r)$ is assumed to decrease linearly with radius. Using equation (B-7), it has the form

$$
\mu(r) = \mu_o\left(1 - 0.17\frac{r}{r_o}\right) \tag{B-24}
$$

where r_o is the outer radius of the crystal. The angle of twist, β, is found by considering the total torque, M, about the cylindrical axis. In terms of cylindrical coordinates (r, θ) in the (x_1, x_2) plane:

$$
M = \int_{r=0}^{r_o} \int_{\theta=0}^{2\pi} \mu(r)\beta r^3 dr d\theta \quad , \tag{B-25}
$$

or

$$
\beta = \frac{M}{(0.22)2\pi\mu_o r_o^4} \tag{B-26}
$$

This stress state can be compared to the homogeneous case for the same total torque M. In the latter situation, the stress state is torsional and:

$$\begin{aligned} T_4 &= \mu_o\beta' x_1 \\ T_5 &= -\mu_o\beta' x_2 \end{aligned} \qquad \text{(B-27)}$$

where

$$\beta' = \frac{M}{(0.25)2\pi\mu_o r_o^4} \quad . \qquad \text{(B-28)}$$

The ratio, T''_4/T_4, is found with the aid of equations (B-26) and (B-28).

$$\frac{T''_4}{T_4} = 1.14\left(1 - 0.17\,\frac{r}{r_o}\right) \qquad \text{(B-29)}$$

T''_4/T_4 decreases linearly from 1.14 at $r = 0$ to 0.945 at $r = r_o$. In the present experiment, one would expect the stress distortion to be less than that indicated by equation (B-29), because the loading rod is certainly non-rigid.

APPENDIX C

INTEGRATION OF THE TORQUE FUNCTION

The torque history at the specimen surface (Figure 5b) can be closely approximated by three separate regions: (1) build-up of torque through the bonding agent to the maximum value, (2) energy loss due to plastic flow, and (3) decay of reflected torque wave through the bond. These three regions are defined by times t_1, t_2, and t_3 in Figure 11.

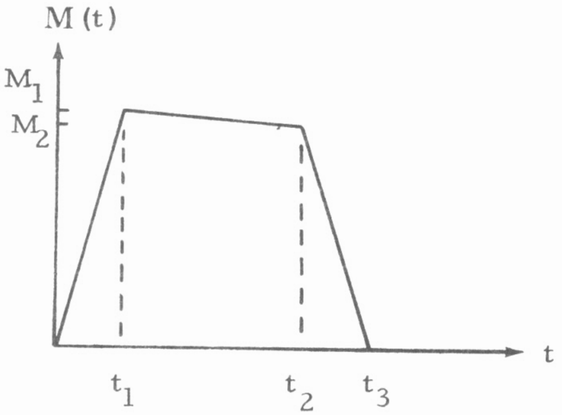

Figure 11. Approximation for the Torque Pulse.

The torque-time relations in the three regions are:

$$M(t) = \frac{M_1}{t_1} t \qquad 0 \le t \le t_1$$

$$M(t) = \frac{(M_1 t_2 - M_2 t_1) - (M_1 - M_2)t}{(t_2 - t_1)} \qquad t_1 < t \le t_2 \qquad \text{(C-1)}$$

$$M(t) = \frac{M_2(t_3 - t\ )}{(t_3 - t_2)} \qquad t_2 < t \le t_3$$

Then:

$$\int_0^{t_3} M^n(t)dt = M_1^n\left(\frac{t_1}{n+1}\right) + \frac{\left(M_1^{n+1} - M_2^{n+1}\right)(t_2 - t_1)}{(M_1 - M_2)(n+1)} + M_2^n\left(\frac{t_3 - t_2}{n+1}\right) . \qquad \text{(C-2)}$$

APPENDIX D

THE INFLUENCE OF THE SHAPE OF A GLIDING DISLOCATION ON DISLOCATION MOBILITY

With reference to Figure 9, and using the requirements of crystal geometry, one can readily show that the torsional stress, resolved on the cross-slip system of dislocation AB, will act in a direction opposed to the dislocation motion. The reverse holds for dislocation segment CD. The magnitude of the resolved shear stress on these segments is 1/3 of that on BC. Hence, AB and CD will inhibit the motion of BC under the influence of the torsional stress. If the edge dislocation BC is much longer than the cross-slipped components (in the experiments BC was of the order of 10^{-2} cm while the height h lay between 0 and 2×10^{-4} cm), then the retarding effect must be small. In any case, the experimentally determined lattice friction force at any dislocation velocity will be an overestimate of the true value. In the following, the magnitude of error as a function of dislocation length, dislocation velocity, and height h is determined.

The dislocation configuration is assumed to move with some equilibrium velocity v in the direction of the Burgers vector $\underline{b}$ through the crystal lattice. Also, it is specified that the lattice friction can be expressed through a damping coefficient B. Then the force per unit length, acting normal to the dislocation line at any point, and in its slip plane, is:

$$\begin{aligned} F_{AB} &= \frac{1}{3}\tau_r b + Bv_n \\ \mathbf{F}_{\mathbf{BC}} &= \tau_r b - Bv_n \qquad \text{(D-1)} \\ F_{CD} &= -\frac{1}{3}\tau_r b + Bv_n \end{aligned}$$

F_{AB}, F_{BC}, and F_{CD} are the normal forces per unit length on the three dislocation segments, and they act in the directions shown in Figure 10. τ_r is the resolved shear stress on BC, and v is the velocity, normal to the dislocation line at any point along its length.

Determination of the dynamic equilibrium configuration of the dislocation is simply a matter of solving the differential equations of equilibrium for the three dislocation segments subject to appropriate boundary conditions. These boundary conditions are defined by the following:

(a) The net force in the direction of the Burgers vector on nodes B and C must be zero.

(b) At points A and D, dislocations AB and CD must be perpendicular to the traces of their glide planes on the free surface.

The schematic representation of dislocation segment AB in Figure 12 is considered.

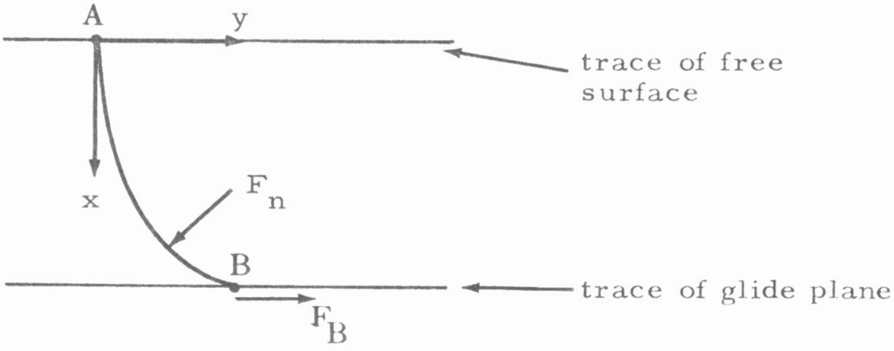

Figure 12. Schematic Representation of Dislocation AB

The coordinate system (x, y) defines the {111} cross-slip plane, and moves with velocity v in the positive y-axis direction. Hence, it is stationary with respect to the dislocation. F_B is the glide force at node B due to dislocation BC.

The shape of the dislocation can be defined by the parameters S and θ, where S refers to the distance along the dislocation from point A and θ is the angle between the dislocation line at any point and the x-axis.

The differential equation of dynamic equilibrium for a small segment dS is (Figure 13):

$$F_n dS = T(\theta) d\theta \tag{D-2}$$

or

$$\frac{1}{3}\tau_r b + Bv\cos\theta = T(\theta)\frac{d\theta}{dS} \tag{D-3}$$

where the effect of the free surface has been omitted.

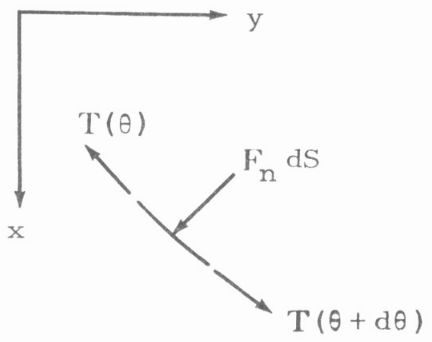

Figure 13. Equilibrium of a Small Segment of Dislocation AB. F_n is the normal force. $T(\theta)$ is the line tension.

For copper, the line tension, $T(\theta)$, is given by [20]:

$$T(\theta) \simeq \frac{b^2}{4\pi}(5.93 - 1.60\sin 2\theta)\ln\frac{r_1}{r_o} \tag{D-4}$$

where r_o and r_1 are appropriate inner and outer cut-off radii for the calculation of line energy. For the present purpose:

$$r_o = 2.5\,b \qquad \text{and} \qquad r_1 = 10^{-3}\ \text{cm} \tag{D-5}$$

are employed.

Differential equations for BC and CD follow immediately. They are, for BC:

$$\tau_r b - Bv\cos\theta = T(\theta)\frac{d\theta}{dS} \tag{D-6}$$

and, for CD:

$$-\frac{1}{3}\tau_r b + Bv\cos\theta = T(\theta)\frac{d\theta}{dS} \tag{D-7}$$

where coordinate systems are defined as before (see Figure 14).

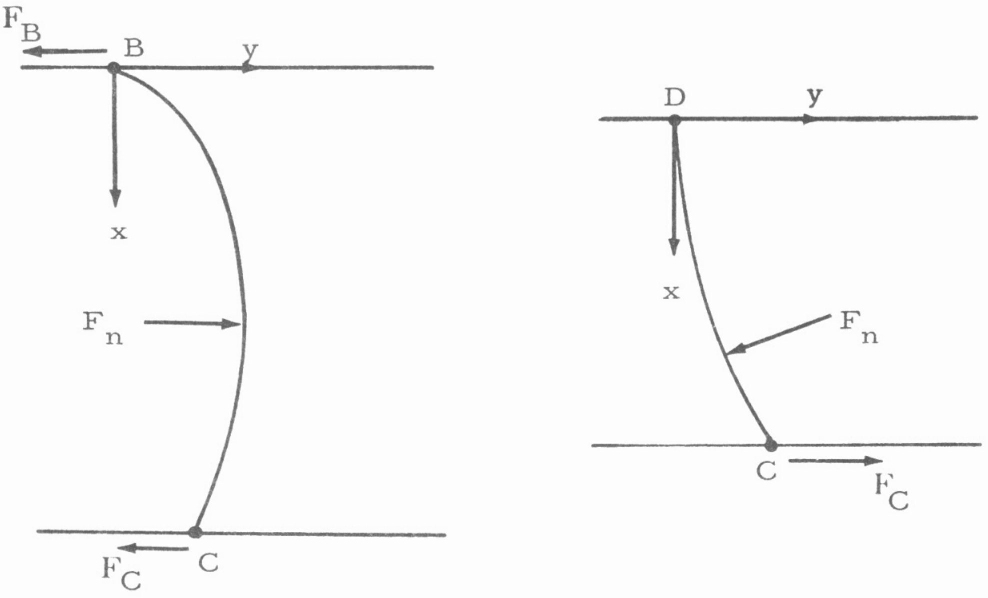

Figure 14. Schematic Representation of Dislocations BC and CD.

Equations (D-3), (D-6), and (D-7) are solved by numerical integration. The procedure follows:

1. A height h, which defines the distance from the primary (111) plane to the free surface, is chosen. Then the maximum distance x along the cross-slip planes is $h/\cos(70.5^\circ)$.

2. A resolved shear stress τ_r is adopted and the corresponding value of v is taken from the experimental data. We are careful to realize that this does not provide the true value of B.
3. A value of B is chosen where the product Bv is less than $\tau_r b$.
4. Equation (D-3) is numerically integrated from point A where the boundary condition is $\theta = 0$, $S = 0$. The integration is stopped when $v = h/\cos(70.5^\circ)$, and $\theta = \theta_{max_{AB}}$.
5. At this point, boundary condition (a) requires that the value of θ at point B in the primary (111) plane equal $(90^\circ - \theta_{max_{AB}})$.
6. Equation (D-7) is numerically integrated from point A as in 4. above. In a manner as before, the value of θ at point C in the primary (111) plane equals $(90^\circ - \theta_{max_{CD}})$.
7. Equation (D-6) is integrated from both ends B and C using the appropriate boundary conditions. Each integration is terminated when $d\theta/dS = 0$. The sum of the two lengths x at this point defines the distance between the cross-slip planes, which we call L.

The calculation for $h = 2 \times 10^{-4}$ cm was carried out for stresses from 1×10^6 to 2×10^7 dynes/cm^2. Overestimation of B was less than 4 percent for values of L greater than 0.01.

The dissipation effect will be less for primary (111) planes closer to the free surface. The maximum error in the experimental results from this cause is then less than 4 percent.

APPENDIX E

THE CONCEPT OF PHONON VISCOSITY

Dislocation mobility in pure copper single crystals as well as in zinc [22, 23] and aluminum [24, 25] is characterized by two important features: (a) the attainment of relatively high velocities for small applied stresses, and (b) decreasing interaction with the crystal lattice with decreasing temperature in the temperature range from about 70°K to 300°K. This dislocation behavior was first proposed theoretically by Leibfried [26], nearly twenty years before direct experimental evidence was available. His model postulated that, in the absence of a large Peierls' barrier, dislocation motion was damped by the interaction of lattice thermal waves with the elastic properties of dislocations. Leibfried specifically considered how dislocation mobility is affected by the stress field of a thermal phonon. This, however, is not the only mechanism to be considered. Since 1950, theories have been put forward to explain thermal phonon-dislocation core and thermal phonon-dislocation strain field interactions. The inherent complexity of the problem has required that many simplifying assumptions be made to obtain estimates of the dislocation drag coefficient as a closed form function of lattice and dislocation properties. While the various theories predict the proper order of magnitude of damping in copper, the experimentally observed temperature dependence of the damping coefficient of edge dislocations in the temperature range from 66°K to 373°K could not be closely approximated by the predictions of one or a combination of mechanisms.

The phonon viscosity theory developed by Mason and others is attractive because it alone predicts the high-temperature behavior (temperatures near the Debye temperature) of the damping coefficient that is experimentally observed. However, the theory has not been worked out in great detail, and there exists some confusion as to the validity of several of its arguments.

The theory itself stems from the original work of Akhieser, who, in a fundamental paper [27], clearly demonstrated the lattice absorption of energy from acoustic (or strain) waves with long wavelengths relative to the thermal phonon mean free path. He reasoned as follows: the thermal phonons are highly localized with respect to the varying strain field; hence, they can be considered as traveling through a uniform medium with a slowly modulating strain field. The lattice thermal frequencies are changed as the result of the impression of the strain, creating temperature differences between phonon modes at any spatial point. The phonons relax to a new thermal equilibrium at some common temperature (adiabatic temperature) through phonon-phonon collisions. Akhieser considered 3-phonon N-process due to anharmonic lattice terms and showed, using the Debye approximation for phonon wave velocities, that the relaxation process was accompanied by an increase of entropy of the system and a corresponding energy absorption from the strain wave.

The temperature change in each phonon mode caused by the Akhieser effect can be calculated as follows. Consider a small instantaneous change in elastic strain impressed upon a crystal initially in thermal equilibrium. The process is adiabatic in the sense of no spatial heat flow. In addition, since the change is instantaneous, it occurs in the absence of phonon - phonon interactions. In equation form:

$$d\langle n_{\underline{q},p}(T)\rangle = \frac{\partial\langle n_{\underline{q},p}(T)\rangle}{\partial\omega}\, d\omega + \frac{\partial\langle n_{\underline{q},p}(T)\rangle}{\partial T}\, dT = 0 \ , \qquad (E.1)$$

where $\langle n_{\underline{q},p}(T)\rangle$ is the phonon occupancy number of mode $(\underline{q}, p)$ at temperature T, and ω is its frequency. In thermal equilibrium:

$$\langle n_{\underline{q},p}(T)\rangle = \frac{1}{\exp(\hbar\omega_{\underline{q},p}/k_B T) - 1} \ , \qquad (E.2)$$

where $\hbar$ is Planck's constant, and k_B is Boltzmann's constant.

and substitution of this value into equation (E.I) gives:

$$\frac{d\omega_{\underline{q},p}}{\omega_{\underline{q},p}} = \frac{dT}{T} \ . \qquad (E.3)$$

The Grüneisen relations [28, 29] require that the phonon frequencies change according to:

$$\omega_{\underline{q},p} = \omega^{o}_{\underline{q},p}\left(1 + \sum_j \gamma^{j}_{\underline{q},p} S_j\right) \ , \qquad (E.4)$$

where $\omega^{o}_{\underline{q},p}$ is the frequency of mode $(\underline{q}, p)$ for the state of no strain, and the $\gamma^{j}_{\underline{q},p}$ are the appropriate Grüneisen numbers. The temperature change for the mode $(\underline{q}, p)$ is then:

$$dT = T\,\frac{\sum_j \frac{\partial\omega_{\underline{q},p}}{\partial S_j}\, dS_j}{\omega_{\underline{q},p}} = \frac{\sum_j \gamma^{j}_{\underline{q},p}\, dS_j}{1 + \sum_j \gamma^{j}_{\underline{q},p} S_j}\, T \qquad (E.5)$$

where the dS_j are the small perturbations in strain. The Grüneisen numbers have different magnitudes, and thus it is obvious that each phonon mode has its unique temperature change. The crystal returns to thermal equilibrium through phonon - phonon interactions governed by the anharmonic terms of the crystal Hamiltonian.

If the strain perturbation is spatially - dependent, then according to equation (E. 5), the temperature change of each phonon mode is a function of position in the crystal. Hence, in the general case, the common equilibrium temperature of the relaxed phonons depends on position in the crystal. This is the so - called adiabatic state [30, 31]. Return to the isothermal condition is now determined by the macroscopic parameters involved in heat flow between spatial points. The energy absorbed from a dislocation strain field in the adiabatic - isothermal transition has been determined exactly [32, 33] and is negligibly small for metals.

In a series of papers, Mason [34, 35], Mason and Bateman [36], and Mason and Rosenberg [37] considered the initial phonon transition and showed that the Akhieser effect was applicable to the absorption of energy from the strain field of a dislocation traveling through an otherwise defect - free crystal lattice. Rather than calculate the entropy produced during the relaxation process described above, they postulated that the elastic stiffnesses of the crystal were altered by the perturbation from equilibrium. They noted that a change in an elastic stiffness multiplied by the time required for the material relaxation was equal to a viscosity, which in turn could be related to energy absorption. The complexity of the situation was therefore reduced to calculation of changes in the elastic stiffnesses at all points in the lattice caused by the strain field of a moving dislocation, and concurrently to find for each an appropriate relaxation time. This has not yet been done on a formal basis, and a critical comparison with experimental results awaits this derivation.

REFERENCES

1. G. A. Alers and D. O. Thompson, "Dislocation Contributions to the Modulus and Damping in Copper at Megacycle Frequencies," J. Appl. Phys. 32, 283 (1961).

2. R. M. Stern and A. V. Granato, "Overdamped Resonance of Dislocations in Copper," Acta Met. 10, 358 (1962).

3. T. Suzuki, A. Ikushima, and M. Aoki, "Acoustic Attenuation Studies of the Frictional Force on a Fast Moving Dislocation," Acta Met. 12, 1231 (1964).

4. K. Marukawa, "Dislocation Motion in Copper Single Crystals," J. Phys. Soc. Jap. 22, 499 (1967).

5. W. F. Greenman, T. Vreeland, Jr., and D. S. Wood, "Dislocation Mobility in Copper," J. Appl. Phys. 38, 3595 (1967).

6. D. P. Pope, T. Vreeland, Jr., and D. S. Wood, "Machine for Producing Square Torsion Pulses of Microsecond Duration," Rev. Sci. Inst. 35, 1351 (1964).

7. D. P. Pope, D. S. Wood, and T. Vreeland, Jr., "Mobility of Edge Dislocations in the Basal-Slip System of Zinc," J. Appl. Phys. 38, 4011 (1967).

8. J. A. Gorman, D. S. Wood, and T. Vreeland, Jr., "Mobility of Dislocations in Aluminum," J. Appl. Phys. 40, 833 (1969).

9. F. W. Young and J. R. Savage, "Growth of Copper Crystals of Low Dislocation Density," J. Appl. Phys. 25, 1917 (1964).

10. J. D. Livingston, "Etch Pits at Dislocations in Copper," J. Appl. Phys. 31, 1071 (1960).

11. D. P. Pope, "The Mobility of Edge Dislocations in the Basal Slip System of Zinc," Ph. D. Thesis, California Institute of Technology, Pasadena, California (1967).

12. A. P. L. Turner, T. Vreeland, Jr., and D. P. Pope, "Experimental Techniques for Observing Dislocations by the Berg-Barrett Method," Acta Cryst. A24, 452 (1968).

13. J. A. Gorman, "The Mobility of Dislocations in High Purity Aluminum," Ph. D. Thesis, California Institute of Technology, Pasadena, California (1968).

14. G. Saada, "Dislocation Interactions and Plastic Deformation of Crystals," Electron Microscopy and Strength of Crystals, Interscience Publishers, New York (1962).

15. A. Granato and K. Lücke, "Theory of Mechanical Damping Due to Dislocations," J. Appl. Phys. 27, 583 (1956).

16. J. P. Hirth and J. Lothe, Theory of Dislocations, McGraw Hill, New York (1968).

17. L. Johnson and M. F. Ashby, "The Stress at Which Dislocations Multiply in Well-Annealed Metal Crystals," Acta Met. 16, 219 (1968).

18. J. S. Koehler and G. deWit, "Influence of Elastic Anisotropy on the Dislocation Contribution to the Elastic Constants," Phys. Rev. 116, 1121 (1959).

19. G. deWit and J. S. Koehler, "Interaction of Dislocations with an Applied Stress in Anisotropic Crystals," Phys. Rev. 116, 1113 (1959).

20. A. K. Head, "The [111] Dislocation in a Cubic Crystal," Phys. Stat. Sol. 6, 461 (1964).

21. R. F. S. Hearmon, Applied Anisotropic Elasticity, Oxford University Press, London (1961).

22. D. P. Pope and T. Vreeland, Jr., to be published.

23. T. Vreeland, Jr. and K. M. Jassby, research in progress, W. M. Keck Laboratory of Engineering Materials, California Institute of Technology, Pasadena, California.

24. J. A. Gorman, D. S. Wood, and T. Vreeland, Jr., "Mobility of Dislocations in Aluminum," J. Appl. Phys. 40, 833 (1969).

25. J. A. Gorman, D. S. Wood, and T. Vreeland, Jr., "Mobility of Dislocations in Aluminum at 74° and 83°K," J. Appl. Phys. 40, 903 (1969).

26. G. Leibfried, "Effect of Thermally Excited Sound Waves on Plastic Deformation," Z. Physik 127, 344 (1950).

27. A. Akhieser, "On the Absorption of Sound in Solids," J. Phys. (USSR) 1, 277 (1939).

28. R. N. Thurston and K. Brugger, "Third-Order Elastic Constants and the Velocity of Small Amplitude Elastic Waves in Homogeneously Stressed Media," Phys. Rev. 133, A1604 (1964).

29. J. M. Ziman, Electrons and Phonons, Oxford University Press, London (1960).

30. M. A. Biot, "Thermoelasticity and Irreversible Thermodynamics," J. Appl. Phys. 27, 240 (1956).

31. K. Lücke, "Ultrasonic Attenuation Caused by Thermoelastic Heat Flow," J. Appl. Phys. 27, 1433 (1956).

32. J. D. Eshelby, "Dislocations as a Cause of Mechanical Damping in Metals," Proc. Roy. Soc. (Lon.) A197, 396 (1949).

33. J. H. Weiner, "Thermoelastic Dissipation Due to High-Speed Dislocations," J. Appl. Phys. 29, 1305 (1958).

34. W. P. Mason, "Phonon Viscosity and Its Effect on Acoustic Wave Attenuation and Dislocation Motion," J. Ac. Soc. Am. 32, 458 (1960).

35. W. P. Mason, "Drag on Dislocations Due to Thermal Losses of the Phonon-Phonon Interaction Type," J. Appl. Phys. 35, 2779 (1964).

36. W. P. Mason and T. B. Bateman, "Ultrasonic-Wave Propagation in Pure Silicon and Germanium," J. Ac. Soc. Am. 36, 644 (1964).

37. W. P. Mason and A. Rosenberg, "Damping of Dislocations in Lead Single Crystals," J. Appl. Phys. 38, 1929 (1967).

38. J. Lothe, "Theory of Dislocation Motion in Pure Slip," J. Appl. Phys. 33, 2116 (1962).